



Nonlinear Free Oscillation of Imperfect FG Porous Stiffened Open Conical Panels Resting on an Elastic Foundation under Thermal Conditions

Vahid Eslamdoust, Habib Ahmadi*

Faculty of Mechanical Engineering, Shahrood University of Technology, Shahrood, Iran.

ABSTRACT: This research examines the nonlinear free oscillations of imperfect functionally graded materials, porous stiffened open conical panels resting on an elastic foundation. The classical shell theory, nonlinear von Kármán-type assumptions, and Hamilton's principle are used to derive the nonlinear dynamic equations. Next, dimensionless parameters are introduced to apply the dimensionless process to the equations of motion. The Galerkin approach is used to discretize the dimensionless partial differential equations. By neglecting in-plane inertia and solving the resulting algebraic equations, the discretized partial differential equations reduce to a nonlinear ordinary differential equation. Using this nonlinear ordinary differential equation, the linear frequencies are extracted, and the numerical results are validated against previous research for various geometries. Furthermore, the multiple scales method is used to extract the nonlinear frequency relationship. Similar to the validation of linear frequencies, the nonlinear frequencies are verified for a geometry reported in previous research. The numerical results are in very good agreement with previous research. Finally, the effects of changes in geometric parameters, material properties, and other influencing factors are reported and discussed using various figures.

Review History:

Received: Nov. 09, 2025

Revised: Jan. 18, 2026

Accepted: Feb. 11, 2026

Available Online: Feb. 21, 2026

Keywords:

Nonlinear Free Vibration

Imperfection

Open Conical Panels

Elastic Foundation

Multiple Scales Method

1- Introduction

Open conical panels (OCPs) are a section of truncated conical shells (TCSs) that, because of their special geometry, are used in many industries, including automotive, aircraft, marine, and aerospace. Therefore, based on these applications, it is necessary to study these structures using various mathematical and engineering approaches. For this purpose, the nonlinear free oscillations of OCPs are studied in this research.

Numerous previous studies have examined the free oscillations of TCSs made of various materials. In this context, Sofiyev et al. [1] studied the free oscillations of non-homogeneous TCSs. Nekouei et al. [2] analyzed the free oscillations of composite TCSs. The governing equations are derived by applying CST and Hamilton's law. Then, the GDQM is used to discretize the PDEs. Javed et al. [3] investigated the free oscillations of composite TCSs with variable thickness using the FSDT. Shekari et al. [4] addressed the free oscillations of rotating sandwich TCSs. The FSDT, Hamilton's law, and Galerkin's approach are employed to obtain and discretize the PDEs. Tong [5] investigated the free vibration of composite TCSs. The governing equations are derived by applying Donnell's assumptions and solved using a power series. Guo et al. [6] studied the free oscillations of composite TCSs using the FSDT, Hamilton's principle,

Walsh series, and the Fourier series. Tong [7] presented the free vibration of orthotropic TCSs using CST and an exact method. Wu et al. [8] examined the free oscillations of orthotropic TCSs resting on a Pasternak medium by applying CST and a domain decomposition approach. Amirabadi et al. [9] reported a free oscillations study of rotating FG-GPL TCSs. The TSDT, Hamilton's principle, and GDQM are applied to establish and discretize the PDEs.

Some previous research has addressed the free vibration of shallow shells and OCPs. In this context, Monterrubio [10] investigated free oscillations of shallow shells using CST and the Rayleigh-Ritz method (RRM). Matsunaga [11] presented the free vibration of FGM shallow shells, using HSDT, Hamilton's law, and Navier's approach. Bardell et al. [12] addressed free oscillations of isotropic OCPs, using CST and FEM to obtain the system's frequency. Akbari et al. [13] examined free oscillations of FGM OCPs, applying FSDT and Hamilton's law to establish the PDEs and using the GDQ approach to discretize them. Zhao et al. [14] studied free oscillations of FGM OCPs, using FSDT and an element-free approach to obtain the natural frequency. Kiani et al. [15] studied free oscillations of FG-CNTRC OCPs, using FSDT, Donnell's assumptions, Hamilton's law, and the Ritz procedure to extract and discretize the fundamental equations. Xiang et al. [16] reported a free oscillations study of FG-CNTRC OCPs, using FSDT, Hamilton's law, and a 2D kernel shape function to obtain and discretize the PDEs. Zhao

*Corresponding author's email: habibahmadif@shahroodut.ac.ir



et al. [17] introduced dynamic analysis and free oscillations of composite TCSs, using FSDT, Hamilton's law, and the Ritz procedure to obtain and solve the PDEs. Wang et al. [18] investigated the free vibration behavior of sandwich TCSs with variable thickness, establishing the PDEs using FSDT and Hamilton's law and discretizing them using the Galerkin approach. Draiche et al. [19] presented a dynamic and static study of FGM doubly curved shells, using HSDT, Hamilton's law, and the Navier solution approach.

Many researchers have studied the forced-vibration analysis of various geometries. In this regard, Mei et al. [20] examined nonlinear forced oscillations of rectangular plates using CST and FEM. Ribeiro [21] investigated forced vibrations of cylindrical shallow shells using HSDT and virtual work. Chakravorty et al. [22] studied forced and free oscillations of shells using FEM. Lei et al. [23] presented a study of forced and free oscillations of GRC-FG cylindrical shells using HSDT, Hamilton's principle, and a frequency-domain procedure. Zhang et al. [24] investigated the forced and free oscillations of an elliptical cylindrical shell. Flügge's shell theory was used to establish the PDEs, and the separation of variables approach was applied to solve them. Qu et al. [25] examined free and forced oscillations of cylindrical shells using HSDT and a domain decomposition approach. Li et al. [26] examined forced oscillations of TCSs using Hamilton's principle and the Rayleigh-Ritz approach. Ma et al. [27] examined forced and free oscillations of coupled TCSs and cylindrical shells using CST and the modified Fourier series. Chen et al. [28] addressed free and forced oscillations of TCSs and cylindrical shells. CST, Flügge's theory, and the power series solution were used. Zaidan and Hasan [29] investigated the dynamic instability of FGP cylindrical panels. FSDT, Hamilton's principle, and the Galerkin approach were used to establish and discretize the PDEs. Sofiyev [30] addressed a frequency study of laminated nanocomposite cylindrical shells subjected to thermal conditions using shear deformation theory. Arshad et al. [31] studied the vibration of bi-layered FGM cylindrical shells. Love's first approximation theory and the RRM were applied to derive and solve the PDEs.

Some researchers have investigated the nonlinear oscillations of plates, cylindrical shells, TCSs, and OCPs. In this context, Woo et al. [32] reported a study of nonlinear free oscillations of FGM plates. The governing equations are derived using CST and solved using the Fourier series. Nanda and Bandyopadhyay [33] investigated nonlinear free oscillations of composite cylindrical shells using FSDT and FEM. Singh et al. [34] examined nonlinear free oscillations of composite shallow shell panels. HSDT, Hamilton's principle, and FEM are applied. Ueda [35] investigated nonlinear free vibrations of TCSs based on Donnell's assumptions and FEM. Jamalabadi et al. [36] examined the nonlinear oscillations of FG-GPL-RC-OCPs resting on elastic foundations. The FSDT, Hamilton's law, and DQM are used to obtain and discretize the fundamental equations. Yang et al. [37] presented the nonlinear dynamic behavior of FGM-TCSs subject to complex loads. The FSDT, Hamilton's principle,

and Galerkin's method are used to establish and simplify the PDEs. Hoa et al. [38] presented the nonlinear behavior of stiffened FG-sandwich-TCSs resting on an elastic medium. The fundamental equations are derived and discretized using CST and Galerkin's approach.

According to previous research, it is observable that few researchers have analyzed the nonlinear free oscillations of OCPs. So, due to the importance and application of OCPs, it is necessary to perform various mechanical analyses of these panels. Therefore, in the context of this study, the nonlinear vibrations study of imperfect stiffened FGP-OCPs is examined for the first time.

The problem is solved by considering the following assumptions: (a) The inner surface of the panel is made of FGM, and the outer surface is made of different porous materials. (b) Stiffeners are placed on the outer and inner surfaces of the panel. (c) The OCP is placed on an elastic foundation. (d) The panel has geometric imperfections. (e) The panel is in a thermal environment. Finally, for the first time, the effects of changes in the semi-vertex angle, the subtended angle, the volume fraction index, different porous materials, stiffeners, temperature, and the amplitude of imperfection are presented and discussed in the form of various figures.

2- Mathematical Modeling of Geometry and Materials

The geometry of conical panels is such that the cross-sectional radius varies along the length. Fig. 1 shows that R_1 and R_2 are the small and large radii, respectively. Also, L , δ , and θ_0 are the length of the OCP, the semi-vertex angle, and the subtended angle.

According to Fig. 1, the coordinate origin is located in the middle plane. The coordinate axes are x , θ , and z . The panel consists of an FGM and a porous material. The FGM properties vary from the porous thickness to the inner surface of the panel, transitioning from metal to ceramic. Metal and ceramic stiffeners are placed on the inner and outer surfaces of the panel, respectively. To simplify modeling, the geometric imperfection is considered similar to the shape function with constant amplitude (for example, Ref. [39]). So, in this paper, similar to some studies, the geometric imperfection is assumed in the form of Eq. (1).

$$w_0(x, \theta) = A \sin\left(\frac{m\pi x}{L}\right) \sin\left(\frac{n\pi\theta}{\theta_0}\right) \quad (1)$$

where m , n , and A are the half-wave numbers and amplitude of imperfection.[39]

2- 1- FG Materials

The properties of FG materials placed on the inner surface of the panel are presented as follows.

$$F = F_c V_c + F_m V_m \quad (2)$$

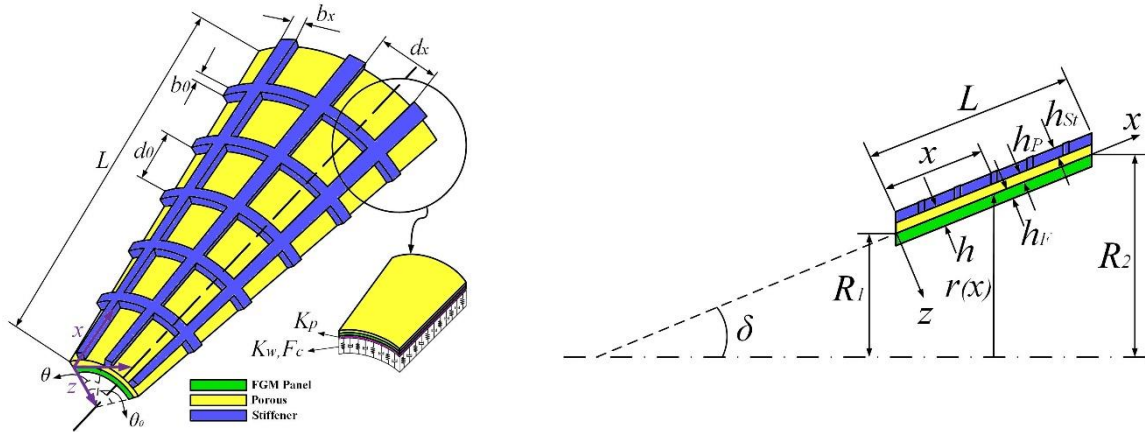


Fig. 1. Conical panel structure.

In the above relationship, V_c and V_m are the volume fraction coefficients, which are formulated in the following form. Also, c and m are indices for ceramic and metal properties, respectively.

$$V_c + V_m = 1 \tag{3}$$

The properties F in Eq. (2) are formulated as follows. [40]

$$F = F_0 (F_{-1}T^{-1} + 1 + F_1T + F_2T^2 + F_3T^3) \tag{4}$$

where F_0 is room temperature and F_{-1}, F_1, F_2, F_3 are known coefficients. The physical properties of the FG material can be calculated utilizing Eq. (2) and Eq. (3) in the following form.

$$E(z) = E_m(1 - V_c) + V_c E_c$$

$$\rho(z) = \rho_m(1 - V_c) + V_c \rho_c$$

$$\alpha(z) = \alpha_m + V_c(\alpha_c - \alpha_m) \tag{5}$$

$$v(z) = V_c(v_c - v_m) + v_m$$

V_c is formulated as follows:

$$V_c = \left(\frac{h - 2z}{2h_{FG}} \right)^k, \quad \frac{h}{2} - h_{FG} \leq z \leq \frac{h}{2} \tag{6}$$

where the volume fraction index is shown by k and $k \geq 0$. [41]

2- 2- Porous Materials

The porous material is placed on the outer surface of the panel. The porous properties are studied in four types. We can formulate these types in the following form. [42]

Type 1: symmetric porosity distribution

$$\rho(z) = \left(1 - N_m \cos\left(\frac{\pi(2z + h - h_p)}{2h_p}\right) \right) \rho_{\max}, \quad -\frac{h}{2} \leq z \leq \frac{-h}{2} + h_p$$

$$G(z) = \left(1 - N_0 \cos\left(\frac{\pi(2z + h - h_p)}{2h_p}\right) \right) G_{\max}, \quad -\frac{h}{2} \leq z \leq \frac{-h}{2} + h_p \tag{7}$$

$$E(z) = \left(1 - N_0 \cos\left(\frac{\pi(2z + h - h_p)}{2h_p}\right) \right) E_{\max}, \quad -\frac{h}{2} \leq z \leq \frac{-h}{2} + h_p$$

Type 2: stiff porosity distribution in the form of non-symmetric

$$\rho(z) = -\rho_{\max} \left(N_m \cos\left(\frac{\pi(2z + h - h_p)}{2h_p}\right) - 1 \right) \tag{8}$$

$$G(z) = -G_{\max} \left(N_0 \cos\left(\frac{\pi(2z + h - h_p)}{2h_p}\right) - 1 \right)$$

$$E(z) = -E_{\max} \left(N_0 \cos\left(\frac{\pi(2z + h - h_p)}{2h_p}\right) - 1 \right)$$

Type 3: soft porosity distribution in the form of non-symmetric

$$\begin{aligned} \rho(z) &= -\rho_{\max} \left(N_m \sin\left(\frac{\pi(2z+h-h_p)}{2h_p}\right) - 1 \right) \\ G(z) &= -G_{\max} \left(N_0 \sin\left(\frac{\pi(2z+h-h_p)}{2h_p}\right) - 1 \right) \\ E(z) &= -E_{\max} \left(N_0 \sin\left(\frac{\pi(2z+h-h_p)}{2h_p}\right) - 1 \right) \end{aligned} \quad (9)$$

Type 4: porosity distribution in the form of uniform

$$\begin{aligned} \rho(z) &= (1 - N_0 \lambda) \rho_{\max} \\ G(z) &= (1 - N_0 \lambda) G_{\max} \\ E(z) &= (1 - N_0 \lambda) E_{\max} \end{aligned} \quad (10)$$

where, the porosity coefficient is denoted by N_0 , which, $0 \leq N_0 \leq 1$. This coefficient is formulated as: $N_0 = 1 - \frac{E_{\min}}{E_{\max}}$ $1 - \frac{G_{\min}}{G_{\max}}$. Also, $N_0 = 1 - \frac{\rho_{\min}}{\rho_{\max}}$, E_{\min} , G_{\min} , and ρ_{\min} are the minimum values of density, shear, and Young's modulus. [42]

In addition, $G(z) = \frac{E(z)}{2(1+\nu)}$, where $E(z)$ is assumed to be constant. The next relationship is presented by Gibson and Ashby, which shows the relation between E and ρ . [42]

$$\frac{E_{\min}}{E_{\max}} = \left(\frac{\rho_{\min}}{\rho_{\max}} \right)^2 \quad (11)$$

N_m and N_0 are formulated based on the above relationships as follows. [42]

$$N_m = -\sqrt{1 - N_0} + 1 \quad (12)$$

Assuming a mass of M for the conical panel, the porosity coefficient of the mass density N_m^* , for a uniform porosity distribution, can be calculated by applying Eq. (11). Then, by utilizing N_m and Eq. (12), the next formula is obtained as follows: [42]

$$N_m^* = \frac{1}{\lambda} - \frac{\sqrt{1 - N_0 \lambda}}{\lambda}; \lambda = \frac{2 N_m}{\pi N_m^*} \quad (13)$$

where λ is uniform porosity, which is indicated as

follows. [42]

$$\lambda = \frac{1}{N_0} - \frac{1}{N_0} \left(1 - \frac{2N_m}{\pi} \right)^2 \quad (14)$$

2- 3- Stiffeners

In this study, the smeared stiffener approach is used to simulate the effect of stiffeners, in which the mechanical properties of stiffeners are distributed, on average and uniformly, over the panel, resulting in equivalent stiffness expressions. The formulation of this method assumes that the stiffeners are perfectly bonded with the panel surface, with no slip at the interface. Also, this model assumed that strain compatibility holds, meaning that there is no relative displacement between the stiffeners and the shell, so they deform together.

As shown in Fig. 1, there are circumferential and longitudinal stiffeners on the inner and outer surfaces of the panel. The number of longitudinal and circumferential stiffeners is defined by n_s and n_θ , respectively. Also, h_x , h_θ , and b_x , b_θ are the thickness and width of the stiffeners in the x and θ directions, respectively. The distance between two circumferential and longitudinal stiffeners is indicated by dx and $d\theta$.

3- Nonlinear theory and stress component

Based on nonlinear von Kármán's assumptions, the strain relations are shown in the following form. [39, 43, 44]

$$\begin{aligned} \epsilon_x^0 &= u_{,x} + \frac{1}{2} w_{,x}^2 + w_{0,x} w_{,x} \\ \epsilon_\theta^0 &= \frac{1}{r(x)} (v_{,\theta} + u \sin(\delta) - w \cos(\delta)) \\ &+ \frac{1}{2r(x)} w_{,\theta}^2 + \frac{1}{r(x)} w_{0,\theta} w_{,\theta} \end{aligned} \quad (15)$$

$$\begin{aligned} \gamma_{x\theta}^0 &= \frac{1}{r(x)} (w_{,x} w_{,\theta} + w_{0,x} w_{,\theta} \\ &+ w_{,x} w_{0,\theta} + u_{,\theta} - v \sin(\delta)) + v_{,x} \end{aligned}$$

$$\kappa_x = -w_{,xx}$$

$$\kappa_\theta = -\frac{1}{r(x)^2} (w_{,\theta\theta} + v_{,\theta} \cos(\delta) - r(x) w_{,x} \sin(\delta)) \quad (16)$$

$$\kappa_{x\theta} = \frac{1}{r(x)^2} \left(\begin{aligned} &2 \sin(\delta) w_{,\theta} - 2 \sin(\delta) w_{,\theta} \\ &+ 2 \sin(\delta) \cos(\delta) v \\ &- r(x) (v_{,x} \cos(\delta) + 2 w_{,x,\theta}) \end{aligned} \right)$$

As we know, the panel radius is variable along the x-direction, which is denoted as follows.

$$r(x) = R_1 + x \sin(\delta), \quad 0 \leq x \leq L \tag{17}$$

By utilizing Eq. (15) and Eq. (16), the strain components are formulated as follows.

$$\varepsilon_x = \varepsilon_x^0 + z \kappa_x, \quad \varepsilon_\theta = \varepsilon_\theta^0 + z \kappa_\theta, \quad \gamma_{x\theta} = \gamma_{x\theta}^0 + z \kappa_{x\theta} \tag{18}$$

So, the strain and stress relationships are written as follows:

$$\begin{aligned} \begin{Bmatrix} \sigma_x^i \\ \sigma_\theta^i \\ \sigma_{x\theta}^i \end{Bmatrix} &= \begin{bmatrix} \mathbf{A}_{11} & \mathbf{A}_{12} & \mathbf{A}_{13} \\ \mathbf{A}_{21} & \mathbf{A}_{22} & \mathbf{A}_{23} \\ \mathbf{A}_{31} & \mathbf{A}_{32} & \mathbf{A}_{33} \end{bmatrix} \begin{Bmatrix} \varepsilon_x \\ \varepsilon_\theta \\ \gamma_{x\theta} \end{Bmatrix} \\ &- \begin{Bmatrix} \mathbf{B}_{11} \\ \mathbf{B}_{21} \\ \mathbf{B}_{31} \end{Bmatrix} \alpha(z, T) \Delta T, \quad i = FG, p \\ A_{11}^i &= A_{22}^i = \frac{E_i(z, T)}{1 - \nu_i^2(z)}, \quad A_{33}^i = \frac{E_i(z, T)}{2(1 + \nu_i(z))} \\ A_{12}^i &= A_{21}^i = \frac{E_i(z, T) \nu_i(z)}{1 - \nu_i^2(z)} \\ A_{13}^i &= A_{23}^i = A_{31}^i = A_{32}^i = 0 \\ B_{11}^i &= \frac{E_i(z, T)}{1 - \nu_i(z)}, \quad B_{21}^i = \frac{E_i(z, T)}{1 - \nu_i(z)}, \quad B_{31}^i = 0 \end{aligned} \tag{19}$$

$$\begin{aligned} \sigma_x^s &= E_x(z, T) \left(\varepsilon_x - \frac{\alpha_x(z, T) \Delta T}{1 - 2\nu(z)} \right), \\ \sigma_\theta^s &= E_\theta(z, T) \left(\varepsilon_\theta - \frac{\alpha_\theta(z, T) \Delta T}{1 - 2\nu(z)} \right), \quad \sigma_{x\theta}^s = 0 \end{aligned}$$

In the thickness direction, two layers of FGM and porous material are stacked on top of each other, with stiffeners on the inner and outer surfaces. As explained in Section 2-3, the stiffeners are treated as layers on the inner and outer surfaces using the smeared stiffener approach. Therefore, to calculate the resultant forces and moments, four integrals must be evaluated for each layer in the thickness direction, and the results added together. Fig. 2 nicely illustrates the bounds of the integrals reported in Eqs. (20) and (23). [43, 44]

The resultants of forces and moments are calculable as follows.

$$\begin{aligned} N_x &= \int_{-\frac{h}{2}}^{-\frac{h}{2}-h_x} \sigma_x^s \frac{b_x}{d_x} dz + \int_{-\frac{h}{2}}^{-\frac{h}{2}+h_p} \sigma_x^p dz \\ &+ \int_{\frac{h}{2}-h_{FG}}^{\frac{h}{2}} \sigma_x^{FG} dz + \int_{\frac{h}{2}}^{\frac{h}{2}+h_x} \sigma_x^s \frac{b_x}{d_x} dz \\ N_\theta &= \int_{-\frac{h}{2}}^{-\frac{h}{2}-h_\theta} \sigma_\theta^s \frac{b_\theta}{d_\theta} dz + \int_{-\frac{h}{2}}^{-\frac{h}{2}+h_p} \sigma_\theta^p dz \\ &+ \int_{\frac{h}{2}-h_{FG}}^{\frac{h}{2}} \sigma_\theta^{FG} dz + \int_{\frac{h}{2}}^{\frac{h}{2}+h_\theta} \sigma_\theta^s \frac{b_\theta}{d_\theta} dz + \\ N_{x\theta} &= \int_{-\frac{h}{2}}^{-\frac{h}{2}+h_p} \sigma_{x\theta}^p dz + \int_{\frac{h}{2}-h_{FG}}^{\frac{h}{2}} \sigma_{x\theta}^{FG} dz \end{aligned} \tag{20}$$

$$\begin{aligned} M_x &= \int_{-\frac{h}{2}}^{-\frac{h}{2}-h_x} \sigma_x^s z \frac{b_\theta}{d_\theta} dz + \int_{-\frac{h}{2}}^{-\frac{h}{2}+h_p} \sigma_x^p z dz \\ &+ \int_{\frac{h}{2}-h_{FG}}^{\frac{h}{2}} \sigma_x^{FG} z dz + \int_{\frac{h}{2}}^{\frac{h}{2}+h_x} \sigma_x^s z \frac{b_\theta}{d_\theta} dz \\ M_\theta &= \int_{-\frac{h}{2}}^{-\frac{h}{2}-h_\theta} \sigma_\theta^s z dz + \int_{-\frac{h}{2}}^{-\frac{h}{2}+h_p} \sigma_\theta^p z \frac{b_\theta}{d_\theta} dz, \\ &\int_{\frac{h}{2}-h_{FG}}^{\frac{h}{2}} \sigma_\theta^{FG} z dz + \int_{\frac{h}{2}}^{\frac{h}{2}+h_\theta} \sigma_\theta^s z dz \\ M_{x\theta} &= \int_{-\frac{h}{2}}^{-\frac{h}{2}+h_p} \sigma_{x\theta}^p z dz + \int_{\frac{h}{2}-h_{FG}}^{\frac{h}{2}} \sigma_{x\theta}^{FG} z dz \end{aligned}$$

By utilizing Eq. (19) and Eq. (20), the following relation is obtained.

$$\begin{aligned} N_x &= A_{10}^x \varepsilon_x^0 + A_{20}^x \varepsilon_\theta^0 + A_{11}^x \kappa_x + A_{21}^x \kappa_\theta - \phi_0^x \\ N_\theta &= A_{20}^\theta \varepsilon_x^0 + A_{10}^\theta \varepsilon_\theta^0 + A_{21}^\theta \kappa_x + A_{11}^\theta \kappa_\theta - \phi_0^\theta \\ N_{x\theta} &= A_{60} \gamma_{x\theta}^0 + A_{61} \kappa_{x\theta} \end{aligned} \tag{21}$$

$$\begin{aligned} M_x &= A_{11}^x \varepsilon_x^0 + A_{21}^x \varepsilon_\theta^0 + A_{12}^x \kappa_x + A_{22}^x \kappa_\theta - \phi_1^x \\ M_\theta &= A_{21}^\theta \varepsilon_x^0 + A_{11}^\theta \varepsilon_\theta^0 + A_{22}^\theta \kappa_x + A_{12}^\theta \kappa_\theta - \phi_1^\theta \\ M_{x\theta} &= A_{61} \gamma_{x\theta}^0 + A_{62} \kappa_{x\theta} \end{aligned} \tag{22}$$

The constant coefficients in the above equations are calculable as follows.

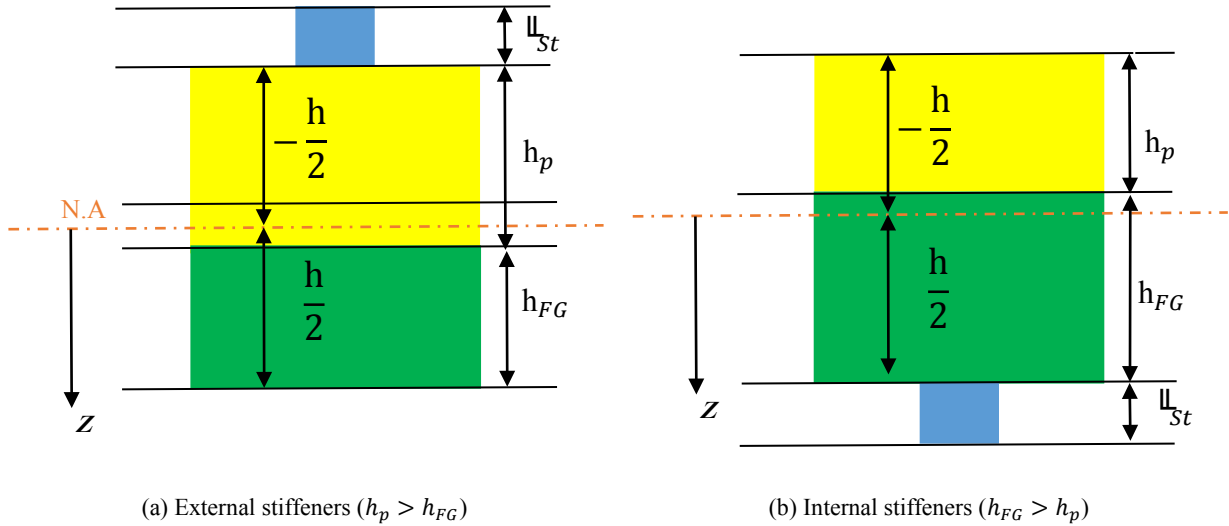


Fig. 2. Stiffened FGP material structure.

$$\begin{aligned}
 A_{li}^x &= \int_{-\frac{h}{2}-h_x}^{-\frac{h}{2}} \frac{E_x(z,T)b_x}{d_x} z^i dz \\
 &+ \int_{-\frac{h}{2}}^{-\frac{h}{2}+h_p} \frac{E^P(z,T)}{1-\nu^2(z)} z^i dz \\
 &+ \int_{\frac{h}{2}-h_{FG}}^{\frac{h}{2}} \frac{E^{FG}(z,T)}{1-\nu^2(z)} z^i dz \\
 &+ \int_{\frac{h}{2}}^{\frac{h}{2}+h_x} \frac{E_x(z,T)b_x}{d_x} z^i dz, i = 0,1,2 \\
 A_{li}^\theta &= \int_{-\frac{h}{2}-h_\theta}^{-\frac{h}{2}} \frac{E_\theta(z,T)b_\theta}{d_\theta} z^i dz \\
 &+ \int_{-\frac{h}{2}}^{-\frac{h}{2}+h_p} \frac{E^P(z,T)}{1-\nu^2(z)} z^i dz \\
 &+ \int_{\frac{h}{2}-h_{FG}}^{\frac{h}{2}} \frac{E^{FG}(z,T)}{1-\nu^2(z)} z^i dz \\
 &+ \int_{\frac{h}{2}}^{\frac{h}{2}+h_\theta} \frac{E_\theta(z,T)b_\theta}{d_\theta} z^i dz, i = 0,1,2 \\
 A_{2i}^x &= A_{2i}^\theta = \int_{-\frac{h}{2}}^{-\frac{h}{2}+h_p} \frac{E^P(z,T)\nu(z)}{1-\nu^2(z)} z^i dz \\
 &+ \int_{\frac{h}{2}-h_{FG}}^{\frac{h}{2}} \frac{E^{FG}(z,T)\nu(z)}{1-\nu^2(z)} z^i dz, i = 0,1,2 \\
 A_{60}^N &= \int_{-\frac{h}{2}}^{-\frac{h}{2}+h_p} \frac{E^P(z,T)}{2(1+\nu(z))} dz \\
 &+ \int_{\frac{h}{2}-h_{FG}}^{\frac{h}{2}} \frac{E^{FG}(z,T)}{2(1+\nu(z))} dz \\
 A_{61}^N &= \int_{-\frac{h}{2}}^{-\frac{h}{2}+h_p} \frac{E^P(z,T)}{(1+\nu(z))} z dz \\
 &+ \int_{\frac{h}{2}-h_{FG}}^{\frac{h}{2}} \frac{E^{FG}(z,T)}{(1+\nu(z))} z dz \\
 A_{61}^M &= \int_{-\frac{h}{2}}^{-\frac{h}{2}+h_p} \frac{E^P(z,T)}{2(1+\nu(z))} z dz \\
 &+ \int_{\frac{h}{2}-h_{FG}}^{\frac{h}{2}} \frac{E^{FG}(z,T)}{2(1+\nu(z))} z dz \\
 A_{62}^M &= \int_{-\frac{h}{2}}^{-\frac{h}{2}+h_p} \frac{E^P(z,T)}{(1+\nu(z))} z^2 dz \\
 &+ \int_{\frac{h}{2}-h_{FG}}^{\frac{h}{2}} \frac{E^{FG}(z,T)}{(1+\nu(z))} z^2 dz \\
 \phi_1^x &= \int_{-\frac{h}{2}-h_x}^{-\frac{h}{2}} \frac{E_x(z,T)\alpha_x(z,T)\Delta T b_x}{d_x} dz \\
 &+ \int_{-\frac{h}{2}}^{-\frac{h}{2}+h_p} \frac{E^P(z,T)\alpha^p(z)\Delta T}{(1-\nu(z))} dz \\
 &+ \int_{\frac{h}{2}-h_{FG}}^{\frac{h}{2}} \frac{E^{FG}(z,T)\alpha(z,T)\Delta T}{1-\nu(z)} dz \\
 &+ \int_{\frac{h}{2}}^{\frac{h}{2}+h_x} \frac{E_x\alpha_x(z,T)\Delta T b_x}{d_x} dz
 \end{aligned}
 \tag{23}$$

$$\begin{aligned}
 \phi_1^\theta &= \int_{-\frac{h}{2}-h_x}^{-\frac{h}{2}} \frac{E_\theta(z, T) \alpha_\theta(z, T) \Delta T b_\theta}{d_\theta} dz \\
 &+ \int_{-\frac{h}{2}}^{-\frac{h}{2}+h_p} \frac{E^P(z, T) \alpha^P(z, T) \Delta T}{(1-\nu(z))} dz \\
 &+ \int_{\frac{h}{2}-h_{FG}}^{\frac{h}{2}} \frac{E^{FG}(z, T) \alpha(z, T) \Delta T}{1-\nu(z)} dz \\
 &+ \int_{\frac{h}{2}}^{\frac{h}{2}+h_\theta} \frac{E_\theta(z, T) \alpha_\theta(z, T) \Delta T b_\theta}{d_\theta} dz \\
 \phi_1^x &= \int_{-\frac{h}{2}-h_x}^{-\frac{h}{2}} \frac{E_x(z, T) \alpha_x(z, T) \Delta T b_x}{d_x} z dz \\
 &+ \int_{-\frac{h}{2}}^{-\frac{h}{2}+h_p} \frac{E^P(z, T) \alpha^P(z, T) \Delta T}{(1-\nu(z))} z dz \\
 &+ \int_{\frac{h}{2}-h_{FG}}^{\frac{h}{2}} \frac{E^{FG}(z, T) \alpha(z, T) \Delta T}{1-\nu(z)} z dz \\
 &+ \int_{\frac{h}{2}}^{\frac{h}{2}+h_x} \frac{E_x(z, T) \alpha_x(z, T) \Delta T b_x}{d_x} z dz \\
 \phi_2^\theta &= \int_{-\frac{h}{2}-h_x}^{-\frac{h}{2}} \frac{E_\theta(z, T) \alpha_\theta(z, T) \Delta T b_\theta}{d_\theta} z dz \\
 &+ \int_{-\frac{h}{2}}^{-\frac{h}{2}+h_p} \frac{E^P(z, T) \alpha^P(z, T) \Delta T}{(1-\nu(z))} z dz \\
 &+ \int_{\frac{h}{2}-h_{FG}}^{\frac{h}{2}} \frac{E^{FG}(z, T) \alpha(z, T) \Delta T}{1-\nu(z)} z dz \\
 &+ \int_{\frac{h}{2}}^{\frac{h}{2}+h_\theta} \frac{E_\theta(z, T) \alpha_\theta(z, T) \Delta T b_\theta}{d_\theta} z dz
 \end{aligned} \tag{23}$$

4- The Fundamental Equations

To establish the fundamental equation, Hamilton’s law is applied as follows.

$$\int_{t_1}^{t_2} (\delta T - \delta U_\varepsilon - \delta W^{nc}) dt = 0 \tag{24}$$

As we know, in the previous formula, T , U , and W^{nc} are kinetic energy, potential energy, and work caused by external excitation, respectively. These terms can be calculated as follows.

$$U_\varepsilon = \frac{1}{2} \int_0^L \int_0^{\theta_0} \begin{bmatrix} N_x \varepsilon_x^0 + M_x \kappa_x \\ + N_\theta \varepsilon_\theta^0 + M_\theta \kappa_\theta \\ + N_{x\theta} \gamma_{x\theta}^0 + M_{x\theta} \kappa_{x\theta} \end{bmatrix} r(x) d\theta dx \tag{25}$$

$$T = \frac{1}{2} \int_0^L \int_0^{\theta_0} I_0 (u_{,t}^2 + v_{,t}^2 + w_{,t}^2) r(x) d\theta dx \tag{26}$$

$$I_0 = \int_{-\frac{h}{2}}^{\frac{h}{2}} \rho(z) dz$$

$$W^{nc} = \frac{1}{2} \int_0^L \int_0^{\theta_0} \begin{bmatrix} K_p (w_{,x}^2 + \frac{1}{x^2 \sin^2(\delta)} w_{,\theta}^2) \\ - K_w w^2 - 2qw \end{bmatrix} r(x) d\theta dx \tag{27}$$

Finally, by replacing Eqs. (25-27) in Eq. (24), the governing equations are obtained in the following form.

$$\begin{aligned}
 H_1 &= N_{x,x} + \frac{1}{r(x)} (\sin(\delta) N_x \\
 &- \sin(\delta) N_\theta + N_{x\theta,\theta}) - I_0 u_{,tt} = 0
 \end{aligned} \tag{28}$$

$$\begin{aligned}
 H_2 &= N_{x\theta,x} + \frac{1}{r(x)} (2 \sin(\delta) N_{x\theta} \\
 &+ N_{\theta,\theta} - \cos(\delta) M_{x\theta}) - \frac{1}{r(x)^2} (2 \cos(\delta) \sin(\delta) M_{x\theta} \\
 &+ \cos(\delta) M_{\theta,\theta}) - I_0 v_{,tt} = 0
 \end{aligned} \tag{29}$$

$$\begin{aligned}
 H_3 &= \frac{1}{r(x)} (w_{,x} \sin(\delta) N_x + w_{0,x} \sin(\delta) N_x \\
 &+ 2N_{x\theta} w_{0,x,\theta} + 2N_{x\theta} w_{,x,\theta} + N_{x\theta,x} w_{,\theta} \\
 &+ N_{x\theta,\theta} w_{,x} + \cos(\delta) N_\theta - \sin(\delta) M_{\theta,x} \\
 &+ 2M_{x\theta,x,\theta} + 2M_{x,x} \sin(\delta)) \\
 &+ \frac{1}{r(x)^2} (w_{,\theta\theta} N_\theta + N_{\theta,\theta} w_{,\theta} \\
 &+ 2 \sin(\delta) M_{x\theta,\theta} + M_{\theta,\theta\theta} + N_\theta w_{0,\theta,\theta}) \\
 &+ N_x w_{0,x,x} + M_{x,xx} + w_{,xx} N_x + N_{x,x} w_{,x} \\
 &+ K_p w_{,xx} + \frac{K_p \sin(\delta) w_{,x}}{r(x)} + \frac{K_p w_{,\theta\theta}}{r(x)^2} - K_w w \\
 &- I_0 w_{,tt} + q = 0
 \end{aligned} \tag{30}$$

The perturbation procedure is applied to compute the nonlinear frequency relationship, so it is common to write the motion equations in a dimensionless form, and the dimensionless parameters are written as follows.

$$\begin{aligned} \bar{u} &= \frac{u}{h}, \quad \bar{w} = \frac{w}{h}, \quad \bar{v} = \frac{v}{h}, \quad \bar{w}_0 = \frac{w_0}{h}, \\ \varepsilon &= \bar{h} = \frac{h}{L}, \quad \bar{x} = \frac{x}{L}, \quad \bar{K} = \frac{K}{EL}, \\ \bar{R}_1 &= \frac{R_1}{L}, \quad \bar{r}(\bar{x}) = \bar{r} = \bar{R}_1 + \bar{x} \sin(\delta), \\ \bar{t} &= \frac{t}{T}, \quad T = \sqrt{\frac{\rho h^2}{E}}, \quad \bar{\omega}_0 = T \omega_0, \quad \bar{\mu} = T \mu \end{aligned} \tag{31}$$

By utilizing the above equation, the PDEs are rewritten in the following form.

$$\bar{H}_1 = B_{11}(\bar{u}) + B_{12}(\bar{v}) + B_{13}(\bar{w}) = 0 \tag{32}$$

$$\bar{H}_2 = B_{21}(\bar{u}) + B_{22}(\bar{v}) + B_{23}(\bar{w}) = 0 \tag{33}$$

$$\begin{aligned} \bar{H}_3 &= B_{31}(\bar{u}) + B_{32}(\bar{v}) + B_{33}(\bar{w}) \\ &+ B_{34}(\bar{u}, \bar{v}, \bar{w}, \bar{w}_0) = 0 \end{aligned} \tag{34}$$

where B_{ij} are differential operators.

5- Discretization of PDEs

The simply supported boundary conditions (SSBCs) are assumed, as shown below. [45]

$$\bar{v} = \bar{w} = \bar{N}_{x\theta} = \bar{M}_x = 0 \quad \text{at} \quad \bar{x} = 0, \bar{x} = 1. \tag{35}$$

$$\bar{u} = \bar{w} = \bar{M}_\theta = \bar{N}_{x\theta} = 0 \quad \text{at} \quad \theta = 0, \theta_0$$

In the case of multi modes, if we consider two or more modes, when the system does not possess an internal resonance, the modes are uncoupled, and we can consider the fundamental mode for the each of mode independently. In this research, it is assumed that the internal resonance dose not occurred. So, due to the above explanation, the fundamental frequency is analyzed for the single mode alone. So, to continue the discretization process, the following equations are used.[45, 46]

$$\bar{u} = \bar{U}(\bar{t}) \cos m\pi\bar{x} \sin\left(\frac{n\pi\theta}{\theta_0}\right) \tag{36}$$

$$\bar{v} = \bar{V}(\bar{t}) \sin m\pi\bar{x} \cos\left(\frac{n\pi\theta}{\theta_0}\right) \tag{37}$$

$$\bar{w} = \bar{W}(\bar{t}) \sin m\pi\bar{x} \sin\left(\frac{n\pi\theta}{\theta_0}\right) \tag{38}$$

$$\bar{w}_0 = \bar{A} \sin m\pi\bar{x} \sin\left(\frac{n\pi\theta}{\theta_0}\right) \tag{39}$$

$$\int_0^1 \int_0^{\theta_0} [\bar{H}_1] \times \cos m\pi\bar{x} \sin\left(\frac{n\pi\theta}{\theta_0}\right) r(x) d\theta d\bar{x} = 0 \tag{40}$$

The values of m and n represent the half-wave number and circumferential wave number in the x and θ direction, respectively. Finally, the Galerkin approach is used to discretize the PDEs as follows.

$$\int_0^1 \int_0^{\theta_0} [\bar{H}_2] \times \sin m\pi\bar{x} \cos\left(\frac{n\pi\theta}{\theta_0}\right) r(x) d\theta d\bar{x} = 0 \tag{41}$$

$$\int_0^1 \int_0^{\theta_0} [\bar{H}_3] \times \sin m\pi\bar{x} \sin\left(\frac{n\pi\theta}{\theta_0}\right) r(x) d\theta d\bar{x} = 0 \tag{42}$$

$$\begin{aligned} L_{101}\bar{U}(\bar{t}) + L_{102}\bar{V}(\bar{t}) + L_{103}\bar{W}(\bar{t}) + L_{104}\bar{W}^2(\bar{t}) \\ + L_{105}\bar{U}_{,\bar{x}\bar{x}}(\bar{t}) + L_{106} = 0 \end{aligned} \tag{43}$$

The resulting discrete form of the PDEs is presented as follows.

$$\begin{aligned} L_{201}\bar{U}(\bar{t}) + L_{202}\bar{V}(\bar{t}) + L_{203}\bar{W}(\bar{t}) \\ + L_{204}\bar{W}^2(\bar{t}) + L_{205}\bar{V}_{,\bar{x}\bar{x}}(\bar{t}) + L_{206} = 0 \end{aligned} \tag{44}$$

$$\begin{aligned} L_{301}\bar{U}(\bar{t}) + L_{302}\bar{V}(\bar{t}) + L_{303}\bar{W}(\bar{t}) \\ + L_{304}\bar{W}^3(\bar{t}) + L_{305}\bar{W}^2(\bar{t}) + L_{306}\bar{W}(\bar{t})\bar{U}(\bar{t}) \\ + L_{307}\bar{W}(\bar{t})\bar{V}(\bar{t}) + L_{308}\bar{W}_{,\bar{x}\bar{x}}(\bar{t}) + L_{309}\bar{K}_p\bar{W}(\bar{t}) \\ + L_{310}\bar{K}_w\bar{W}(\bar{t}) + L_{311} + L_{312}q = 0 \end{aligned} \tag{45}$$

$$\alpha^* \bar{W}_{,\bar{x}\bar{x}}(\bar{t}) + \alpha_1^* \bar{W}(\bar{t}) + \alpha_2^* \bar{W}^2(\bar{t}) + \alpha_3^* \bar{W}^3(\bar{t}) = \alpha_q \bar{q} \tag{46}$$

In the above formula, the L_{ijk} coefficients are constant terms, which are presented in the Appendix A .

In Eqs. (43) and (44), by ignoring the in-plane inertias and solving the linear equations based on \bar{W} , we can derive \bar{U} and \bar{V} . Then, by substituting \bar{U} and \bar{V} in Eq. (45), a Non-

linear-ODE is established in the following form.

$$\bar{q} = \frac{1}{\alpha_q} (\alpha_1^* \bar{W}(\bar{t}) + \alpha_2^* \bar{W}^2(\bar{t}) + \alpha_3^* \bar{W}^3(\bar{t})) \quad (47)$$

To investigate the bulking analysis, first, neglecting the inertial term in the above relation, we can write:

$$\bar{W}_{,\bar{t}\bar{t}}(\bar{t}) + \alpha_1 \bar{W}(\bar{t}) + \alpha_2 \bar{W}^2(\bar{t}) + \alpha_3 \bar{W}^3(\bar{t}) = 0 \quad (48)$$

To calculate the static critical bulking load, we should solve the equation as $\frac{d\bar{q}}{d\bar{w}} = 0$. The results of this analysis are presented in the next session in Table 6.

By neglecting the external load, Eq. (46) can be rewritten as follows.

$$\bar{\omega}_0 = \sqrt{\alpha_1} \quad (49)$$

where α_1 , α_2 , and α_3 are reported in Appendix B.

Finally, the natural frequency is calculated according to the following equation.

$$\ddot{u} + \bar{\omega}_0^2 u + \alpha_2 \varepsilon u^2 + \alpha_3 \varepsilon^2 u^3 = 0 \quad (50)$$

6- Non-linear Frequency

The MSM is used to extract the nonlinear frequency relationship. To continue the frequency analysis, $\bar{W}(\bar{t})$ is treated as an order of εu , where ε is expressed as a ratio ($\varepsilon = O\left(\frac{h}{l}\right)$) in Eq. (31). So, Eq.(48) is then rewritten as follows.[47]

$$u(\bar{t}; \varepsilon) = u_0(T_0, T_1, T_2) + \varepsilon u_1(T_0, T_1, T_2) + \varepsilon^2 u_2(T_0, T_1, T_2) \quad (51)$$

The system response is considered based on the MSM in the following form.

$$D_0^2 u_0 + \bar{\omega}_0^2 u_0 = 0 \quad (52)$$

where T_0 , T_1 and T_2 are multiple time variables ($T_n = \varepsilon^n t, n = 1, 2, 3, \dots$).

By replacing Eq. (51) into Eq. (50) and sorting the result by order of ε , the coefficients of ε^0 , ε^1 , and ε^2 are

extracted as follows.

$$D_0^2 u_1 + \bar{\omega}_0^2 u_1 = -2D_0 D_1 u_0 - \alpha_2 u_1^2 \quad (53)$$

$$D_0^2 u_2 + \bar{\omega}_0^2 u_2 = -2D_0 D_1 u_2 - D_1^2 u_1 - 2D_0 D_2 u_1 - 2\alpha_2 u_1 u_2 - \alpha_3 u_1^3 \quad (54)$$

$$u_0 = A(T_1, T_2) e^{(i\bar{\omega}_0 T_0)} + \bar{A}(T_1, T_2) e^{(-i\bar{\omega}_0 T_0)} \quad (55)$$

By solving Eq. (52), the general solution is obtained as follows.

$$u_1 = \frac{\alpha_2 A^2}{3\bar{\omega}_0} e^{(2i\bar{\omega}_0 T_0)} - \frac{\alpha_2}{\bar{\omega}_0} A \bar{A} + cc \quad (56)$$

By substituting the above relation into Eq. (53), the secular terms are extracted and must be zero. From this outcome, we conclude that $A = A(T_2)$. Using this result, the particular solution of Eq. (53) is obtained as follows.

$$D_0^2 u_2 + \bar{\omega}_0^2 u_2 = - \left[2i \bar{\omega}_0 D_2 A - \frac{10\alpha_2^2 - 9\alpha_3 \bar{\omega}_0^2}{3\bar{\omega}_0^2} A^2 \bar{A} \right] e^{(i\bar{\omega}_0 T_0)} - \frac{2\alpha_2^2 + 3\alpha_3 \bar{\omega}_0^2}{3\bar{\omega}_0^2} A^3 e^{(3i\bar{\omega}_0 T_0)} + cc \quad (57)$$

where cc denotes the complex conjugate terms.

Using Eqs. (55) and (56), Eq. (54) can be rewritten as follows.

$$\left[2i \bar{\omega}_0 D_2 A - \frac{10\alpha_2^2 - 9\alpha_3 \bar{\omega}_0^2}{3\bar{\omega}_0^2} A^2 \bar{A} \right] = 0 \quad (58)$$

The secular term in the above formula must be zero. Thus, we have:

$$A(T_2) = \frac{1}{2} a(T_2) e^{(i\beta(T_2))}, \bar{A}(T_2) = \frac{1}{2} a(T_2) e^{(-i\beta(T_2))} \quad (59)$$

In the above equation, A and \bar{A} are expressed in polar form, as shown in the following relations.

$$a'\bar{\omega}_0 = 0, \bar{\omega}_0 a \beta' + \frac{10\alpha_2^2 - 9\alpha_3 \bar{\omega}_0^{-2}}{24\bar{\omega}_0} a^3 = 0 \quad (60)$$

By replacing Eq. (59) into Eq. (58) and separating the result into real and imaginary parts, the following relationships are obtained.

$$A = \frac{1}{2} e^{(i \frac{9\alpha_3 \bar{\omega}_0^{-2} - 10\alpha_2^2}{24\bar{\omega}_0} a^2 \varepsilon^2 t + i \beta_0)}, \quad (61)$$

$$\bar{A} = \frac{1}{2} e^{(-i \frac{9\alpha_3 \bar{\omega}_0^{-2} - 10\alpha_2^2}{24\bar{\omega}_0} a^2 \varepsilon^2 t - i \beta_0)}$$

By solving the above relations, a and β are established. Then, by replacing the results into Eq. (59) and using $T_n = \varepsilon^n t$, the following formula is obtained.

$$u = a\varepsilon \cos(\bar{\omega}_{NL} t + \beta_0) - \frac{a^2 \varepsilon^2 \alpha_2}{2\alpha_1} [1 - \frac{1}{3} \cos(2\bar{\omega}_0 t + 2\beta_0)] + O(\varepsilon^3) \quad (62)$$

By replacing Eq. (62) into Eq. (58), the particular solution is obtained. Substituting this result, Eq. (55), and Eq. (56) into Eq. (51), the system response is obtained as follows.

$$\bar{\omega}_{NL} = \bar{\omega}_0 [1 + \frac{9\alpha_3 \alpha_1 - 10\alpha_2^2}{24\alpha_1^2} a^2 \varepsilon^2] \quad (63)$$

where $\bar{\omega}_{NL}$ is given by.

$$\bar{\omega}_d = \bar{\omega}_{NL} - \bar{\omega}_0 \rightarrow \sigma = \frac{\bar{\omega}_{NL}}{\bar{\omega}_0} - 1 \quad (64)$$

By performing the following calculations, the above equation is rewritten in the form of Eq. (65).

$$\bar{\sigma} = [\frac{9\alpha_3 \alpha_1 - 10\alpha_2^2}{24\alpha_1^2} a^2 \varepsilon^2] \quad (65)$$

$$m = 1, k = 1, \delta = 45^\circ, \theta_0 = 80^\circ,$$

$$h = 0.004 \text{ m}, R_2 = 100h, L = \frac{R_2}{4 \sin(\delta)}, \quad (66)$$

$$R_1 = R_2 - L \sin(\delta), T = 300^\circ \text{ K},$$

$$h_F = 0.5 \times h, h_p = 0.5 \times h,$$

$$v_c = v_m = 0.3, N_0 = 0.5, h = h_{FG} + h_p$$

7- Numeric Outcomes

To perform numerical simulation, the geometric and material properties are presented in Eq. (66) and Table 1, respectively. Using SSBCs, the equations are solved, and the numerical solutions for conical panels, conical shells, and rectangular plates are presented in Tables 2-5. Table 2 compares the natural frequency parameters for the homogeneous conical shell. Table 3 presents the first eight natural frequency parameters for the conical panel. Table 4 addresses the non-dimensional frequency for rectangular plates. Table 5 investigates the nonlinear to linear frequency ratio for square plates. As shown, the numerical results are in close agreement with previous research. Also, Table 6 presents the static critical load for the FG-open conical panel.

To better understand the system's behaviour, it is necessary to examine the natural frequencies, because in the next section, the fundamental frequency will serve as the basis for the representative figures. In this study, natural frequencies are calculated for different (m, n) using Eq. (47). Figure 3 illustrates the variation of the first sixty natural frequencies of the system. We observe that the smallest natural frequency for the system occurs for $(1, 3)$.

Table 1. FGM properties.[48]

Coefficients	Ceramic: Si_3N_4			Metal: $SUS304$		
	E_c (Pa)	ρ_c ($\frac{kg}{m^3}$)	α_c	E_m (Pa)	ρ_m ($\frac{kg}{m^3}$)	α_m
F_0	348.43×10^9	2370	5.87×10^{-6}	201.04×10^9	8166	12.33×10^{-6}
F_{-1}	0	0	0	0	0	0
F_1	-3.07×10^{-4}	0	9.095×10^{-4}	3.079×10^{-4}	0	8.086×10^{-4}
F_2	2.16×10^{-7}	0	0	-6.534×10^{-7}	0	0
F_3	-8.946×10^{-11}	0	0	0	0	0
F	3.2227×10^{11}	2370	7.4716×10^{-6}	2.0779×10^{11}	8166	1.5321×10^{-5}

Table 2. Comparison of natural frequency parameters ($f = \omega R_2 \sqrt{\frac{(1-\mathcal{G}^2)\rho_m}{E_m}}$) for SS homogenous conical shell.

n	Present	[49]	[9]	[50]	[51]	[52]
2	0.6704	0.6546	0.6694	0.6309	0.6310	0.6310
3	0.5266	0.5133	0.5425	0.5061	0.5065	0.5062
4	0.4149	0.4079	0.4562	0.3941	0.3947	0.3942
5	0.3448	0.3464	0.4084	0.3337	0.3348	0.3340
6	0.3261	0.3286	0.3955	0.3235	0.3248	0.3239
7	0.3444	0.3485	0.4132	0.3510	0.3524	0.3514
8	0.3932	0.3972	0.4554	0.4019	0.4033	0.4023
9	0.4635	0.4665	0.5157	0.4671	0.4684	0.4676

Table 3. First eight natural frequency parameters ($f = \frac{\omega L^2 h^{-1}}{2\pi} \sqrt{\frac{\rho_c}{E_c}}$) for SS FGM conical panel (material Al/ZrO2).

$R_1 = 0.2 \text{ m}, h = 0.01 \text{ m}, L = 0.8 \text{ m}, \delta = 60^\circ, \theta_0 = 120^\circ$

k		f_1	f_2	f_3	f_4	f_5	f_6	f_7	f_8
0	[14]	3.2521	3.5759	3.9732	5.0811	5.7963	6.2338	6.3819	6.4761
	[13]	3.2749	3.6031	4.0151	5.1564	5.8230	6.2824	6.4260	6.5952
	Present	3.1135	3.8104	4.0361	5.4150	5.6189	6.3415	6.4563	6.6177
0.5	[14]	2.9521	3.2801	3.5905	4.5798	5.3319	5.6706	5.8280	5.8469
	[13]	2.9723	3.3031	3.6275	4.6465	5.3564	5.7140	5.8854	5.9351
	Present	2.7783	3.2812	3.6356	4.6099	4.9567	5.6492	5.6960	5.7883
1	[14]	2.8123	3.1231	3.4215	4.3649	5.0762	5.4018	5.5546	5.5682
	[13]	2.8321	3.1454	3.4575	4.4295	5.0998	5.444	5.6051	5.6585
	Present	2.5642	2.9859	3.3772	4.1707	4.5400	5.1847	5.2187	5.3615
5	[14]	2.5764	2.7945	3.1688	4.0679	4.5052	4.9259	4.9933	5.1946
	[13]	2.5949	2.8143	3.2029	4.129	4.5261	4.9651	5.0281	5.2913
	Present	2.1000	2.5379	3.5859	3.7078	4.1378	4.4036	4.7292	5.2908
10	[14]	2.5012	2.7051	3.0804	3.9573	4.3563	4.7797	4.8349	5.0551
	[13]	2.5193	2.7242	3.1137	4.0169	4.3765	4.8178	4.8687	5.1496
	Present	1.9578	2.4348	2.4348	3.4468	4.2060	4.9699	4.9847	5.1021

Table 4. Compression of frequency parameters of an isotropic rectangular plate. ($f = \omega\alpha^2 \sqrt{\frac{\rho h}{D}}$)

$\nu = 0.3, R_1 = 100 \text{ m}, h = 0.01 \text{ m}, L = 0.1 \text{ m}, \delta = 0.001 \text{ rad}, \theta_0 = 0.001 \text{ rad}$			$\nu = 0.3, R_1 = 100 \text{ m}, h = 0.01 \text{ m}, L = 0.1 \text{ m}, \delta = 0.001 \text{ rad}, \theta_0 = 0.0004 \text{ rad}$				
(m, n)	$\frac{a}{b} = 1$		(m, n)	$\frac{a}{b} = 2.5$			
	[53]	[54]		[53]	[54]	Present	
(1,1)	19.739	19.739	19.7392	(1,1)	71.555	71.555	71.5554
(1,2)	49.348	49.348	49.3480	(2,1)	101.163	101.163	101.1634
(2,1)	49.348	49.348	49.3480	(3,1)	150.511	150.511	150.5114
(2,2)	78.957	78.957	78.9568	(4,1)	219.599	219.599	219.5986
(1,3)	98.696	98.696	98.6960	(1,2)	256.610	256.610	256.6097
(3,1)	98.696	98.696	98.6960	(2,2)	286.219	286.219	286.2185

Table 5. Compression of the nonlinear to linear frequency ratio of an isotropic square plate.

$\frac{w_{\max}}{h}$	0.2	0.4	0.6	0.8	1
[55]	1.023	1.090	1.192	1.321	1.468
[56]	1.028	1.104	1.220	1.364	1.527
[57]	1.033	1.129	1.280	1.453	1.658
[54]	1.033	1.127	1.268	1.443	1.640
Present	1.0281	1.1125	1.2531	1.4500	1.7031

Table 6. Static critical load for the FG-open conical panel. ($h_{FG} = 0.004 \text{ m}$).

ΔT	δ_0			
	30°	45°	60°	75°
75°	868303 Pa	573261	251109	83702
100	781467	447017	170239	45345
120	710681	344176	104369	14104

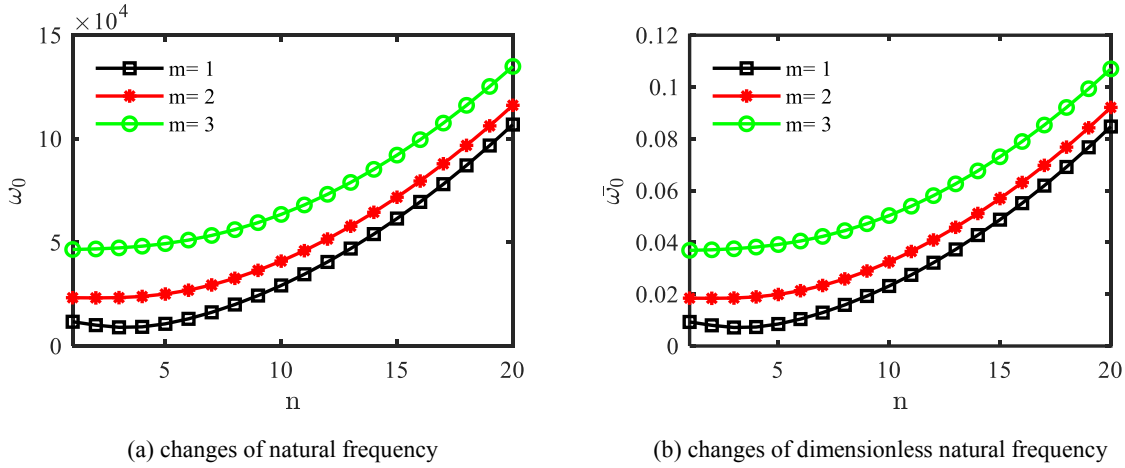


Fig. 3. Effect of the first sixty natural frequency changes based on the circumferential wave number (n).

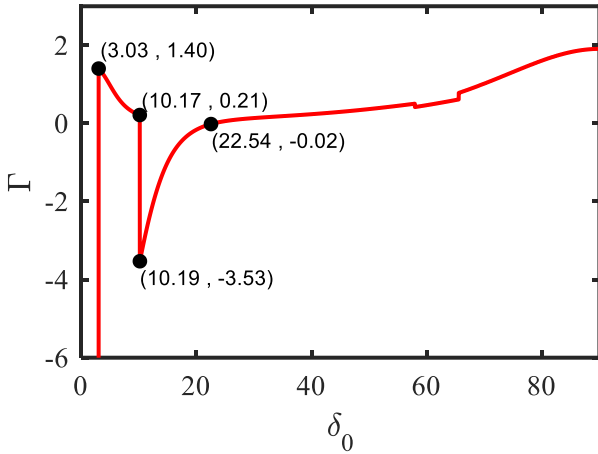


Fig. 4. Effect of changes in the semi-vertex angle on Γ

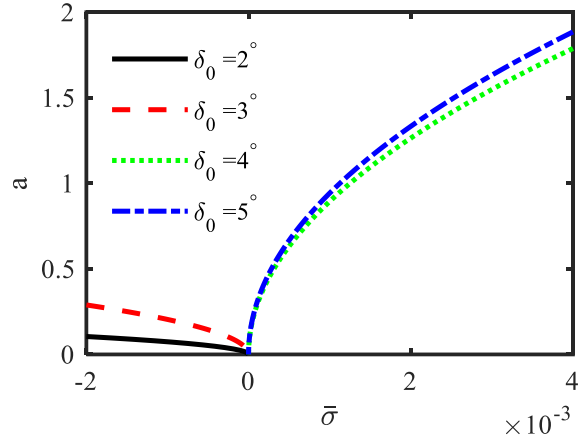


Fig. 5. Semi-vertex angle changes.

8- Simulation Outcomes of Stiffened FGP-OCs

In this part, the results of the various geometrical and physical parameters of the backbone curve for the fundamental mode ($m = 1, n = 3$) are investigated. To better understand the presented results, we define the Γ in Eq. (67) as follows.

$$\Gamma = \frac{9\alpha_3\alpha_1 - 10\alpha_2^2}{24\alpha_1^2} \tag{67}$$

By changing any of the material or geometric parameters in the system, the Γ value can become positive or negative. The system exhibits softening behavior when Γ is negative ($10\alpha_2^2 > 9\alpha_1\alpha_3$). The system exhibits hardening behavior

when Γ is positive ($10\alpha_2^2 < 9\alpha_1\alpha_3$). In this regard, Fig. 4 examines the effect of changes in the Γ parameter. We observe that for angles less than 3° and between 11° and 22° , this value is negative, so in these ranges, the behavior of the system is softening.

Fig. 5 and 6 confirm the previous discussion. We observe that, as the semi-vertex angle increases, the system's behavior transitions between hardening and softening states. For $\delta_0 < 4^\circ$ and $11^\circ \leq \delta_0 \leq 22^\circ$, the system behavior is softening. Outside these ranges, up to $\delta_0 = 90^\circ$, the system behavior increases. Physically, as this parameter increases, the panel becomes wider and closer to a flat plate. So, during vibration, the membrane strains, which are inherently stiffening, become larger.

As in the previous case, to examine how increasing the

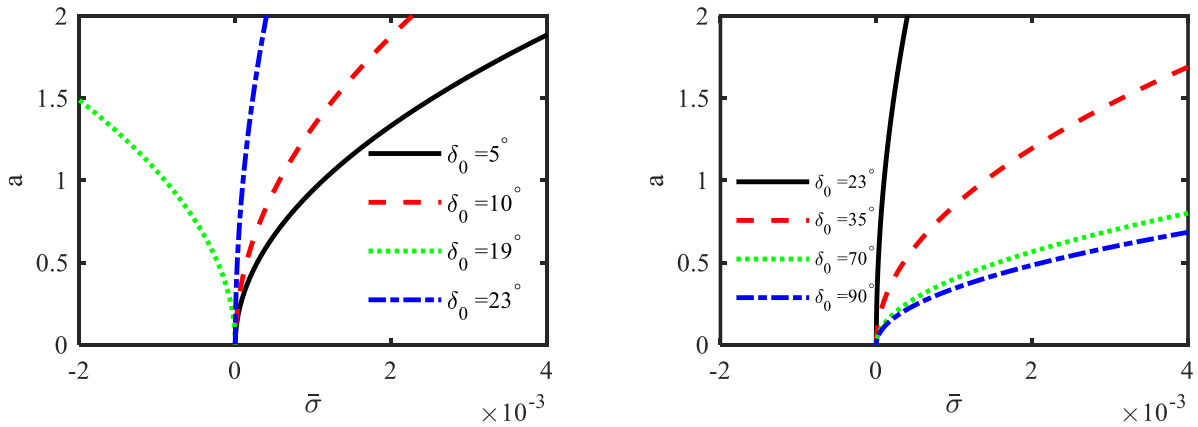


Fig. 6. Semi-vertex angle changes.

subtended angle affects the system’s behavior, it is necessary to analyze the Γ diagram. Based on Fig. 7 and Fig. 8, it is observed that when $\theta_0 \leq 15^\circ$, the Γ value is maximum and positive, so the system is expected to exhibit hardening behavior in this range. When $15^\circ < \theta_0 \leq 29^\circ$, the Γ value is negative, and the system exhibits softening behavior. As the subtended angle increases to 37° , the hardening behavior increases, and for $37^\circ \leq \theta_0 \leq 360^\circ$, the behavior remains hardening, but the value decreases.

Fig. 8 shows the effect of subtended angle changes on system behavior. As shown, for $\theta_0 \leq 15^\circ$, the effect of membrane stresses is high, so the system behavior is hardening. For $15^\circ \leq \theta_0 \leq 29^\circ$, the effect of membrane stresses is minimal and negative, and the system behavior is softening. Finally, for $\theta_0 \geq 19^\circ$, membrane stresses increase, and the system behavior gradually becomes hardening.

Fig. 9 shows how changes in the volume fraction index affect \tilde{A} and the backbone curve. As shown, the hardening behavior increases slightly, $0 \leq k \leq 0.44$, and then decreases with increasing k . The initial increase in hardening behavior is attributed to the ceramic phase’s dominant contribution, which has a high elastic modulus relative to the metal phase, resulting in increased effective stiffness and membrane stresses. For $k > 0.44$, the ceramic phase’s brittle properties become dominant, reducing the metal matrix’s ability to uniformly distribute stress and absorb energy and reducing the effective dynamic stiffness, which in turn reduces the vibrational hardening behavior of the system.

Fig. 10 shows the effect of Γ changes as a function of the porosity coefficient. It can be seen that increasing this coefficient reduces gamma and the system’s hardening behavior. Physically, increasing this coefficient, due to increased microstructure in the material, reduces the material’s elastic modulus and effective stiffness. Therefore, geometric nonlinearity is reduced, and the system’s dynamic behavior becomes softer.

Fig. 11, which illustrates how changes in the porous coefficient affect system behavior for different porous

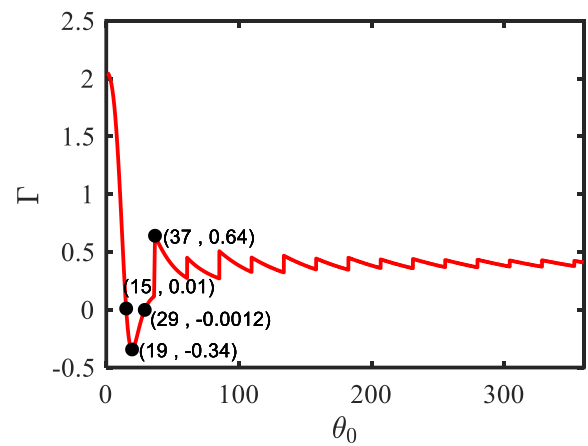


Fig. 7. Effect of changes in the subtended angle on Γ

material types, strongly confirms the previous discussion. According to the figure, we observe that with the increase of this parameter cause to reduce the hardening behavior. The influence of different types of porous material can be attributed mainly to their structural and mechanical properties. Each type of porous material has a unique arrangement and size that affects the distribution and transport of stress through materials. These changes affect the dynamic properties, such as elastic modulus, resulting in different responses under load conditions.

Fig. 12 shows the effect of thickness changes. As the thickness of the porous material increases, the ability to store strain energy decreases because of porosity, so the effective modulus and flexural stiffness of the structure decrease. However, increasing the thickness of functionally graded materials results in greater hardening behavior because of their greater ability to deform and store energy. Therefore, as the porous thickness increases, the hardening effect is

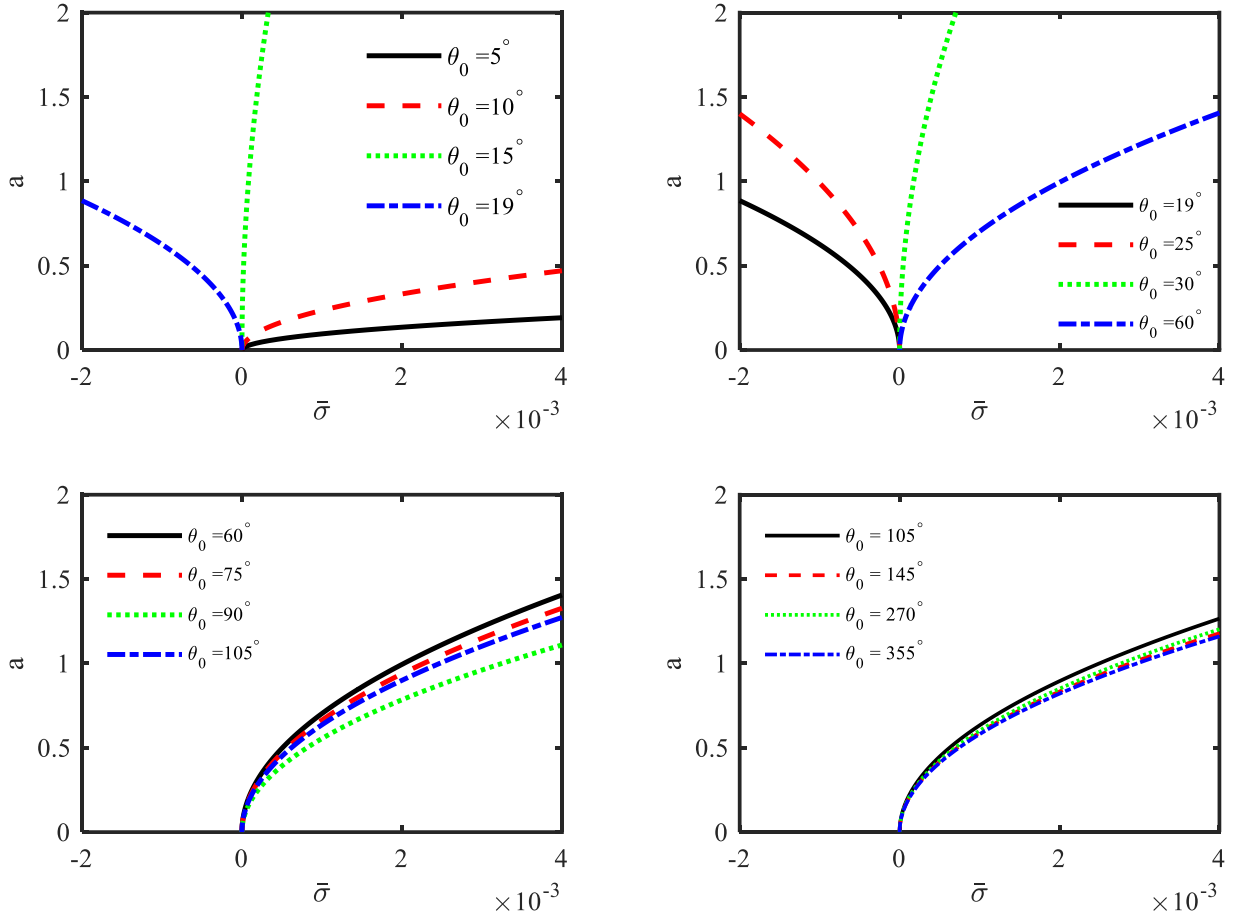


Fig. 8. Effect of subtended angle changes.

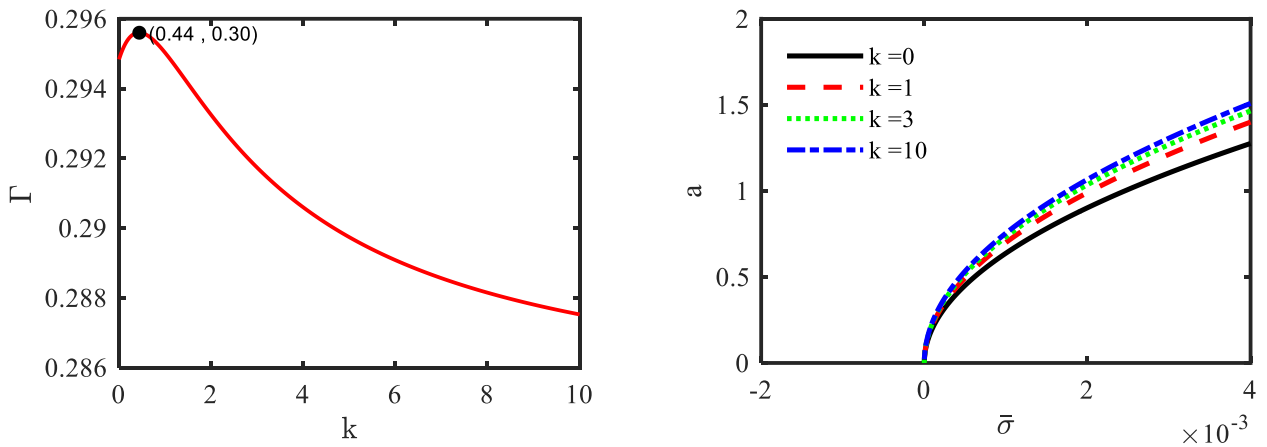


Fig. 9. Effect of volume fraction index changes on Γ and backbone curve.

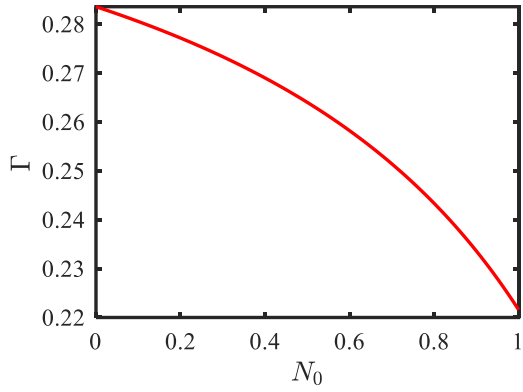


Fig. 10. Effect of changes in the subtended angle on Γ .

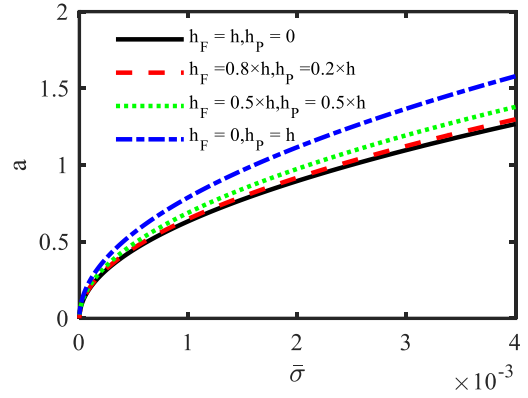
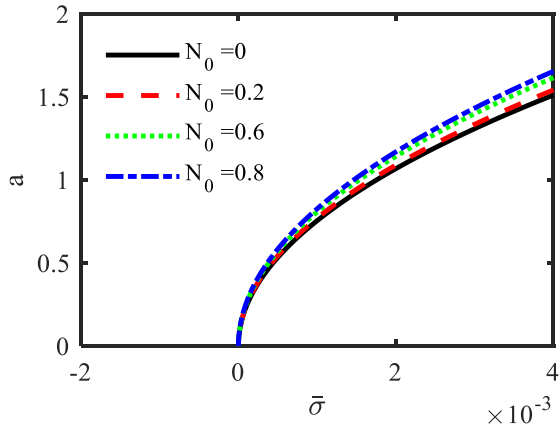
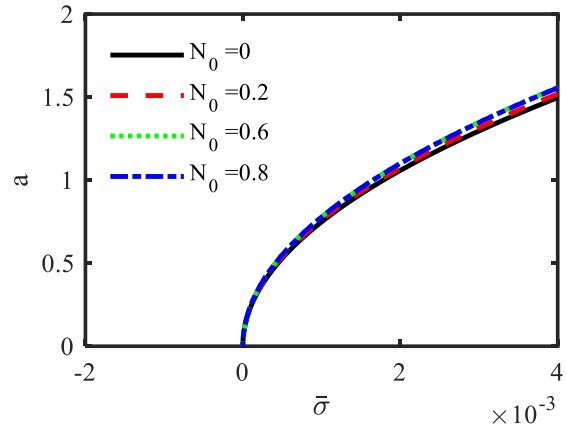


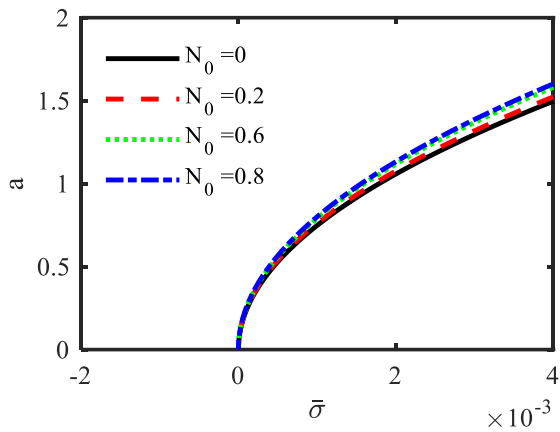
Fig. 12. Effect of porous thickness.



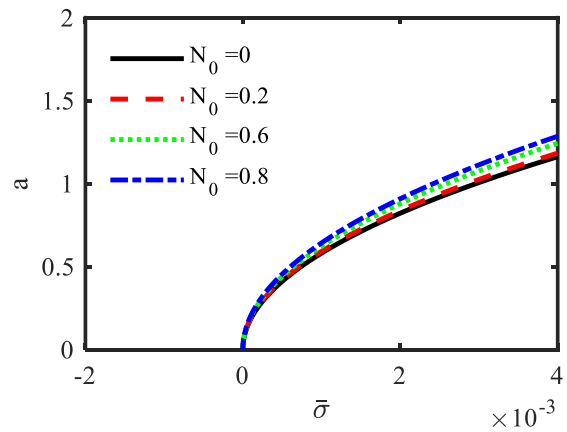
Type1



Type2



Type3



Type4

Fig. 11. Effect of porous type changes.

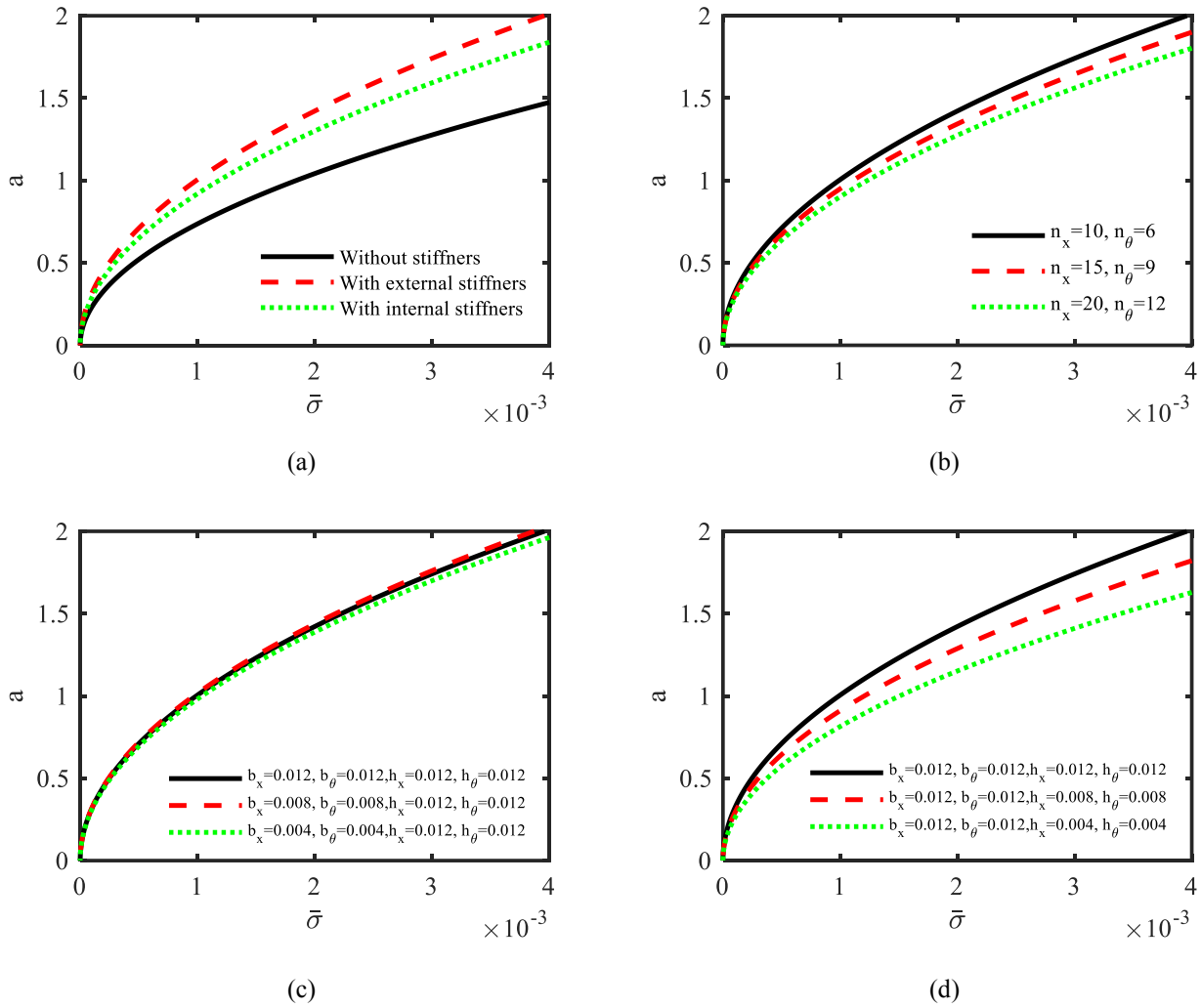


Fig. 13. Effect of stiffener.

reduced, and the system behavior becomes softer.

Fig. 13 shows the effect of stiffeners on the nonlinear system vibrations. Stiffeners can change the stiffness distribution and the force transmission path. Adding them to the system reduces flexibility and shifts stiffness concentration because part of the vibrational energy is absorbed by them. However, increasing their number and thickness increases stiffness and limits larger deformations, resulting in increased vibrational hardening behavior.

Fig. 14 shows the effect of elastic foundation coefficients. As we see, part of the system’s vibration energy is absorbed by the elastic foundation, which distributes the deformations between the panel and the elastic medium and reduces the concentration of strain energy in the panel. So, the hardening behavior is reduced.

Fig. 15 shows the effect of temperature on the system behavior, indicating that the behavior changes from hardening to softening as the temperature increases. Physically, the

elastic modulus and mechanical strength of materials decrease with increasing temperature. At high temperatures, interatomic bonds weaken due to atomic vibrations and greater molecular motion, and the effective stiffness of the system decreases. These changes cause the curve to shift to the right and the behavior of the system to soften.

Fig.16 illustrates the effect of changes in imperfection amplitude. At small initial geometric imperfection amplitudes, the system is in a nearly symmetrical state, so increasing the amplitude causes an increase in the effective stiffness and hardening behavior. However, as the amplitude increases, a large portion of the vibration energy is spent on opening and closing this deformation, so the effective stiffness decreases, and the system behavior becomes softening.

9- Conclusion

In this study, utilizing classical theory, Hamilton’s principle, and Galerkin’s method, equilibrium equations for

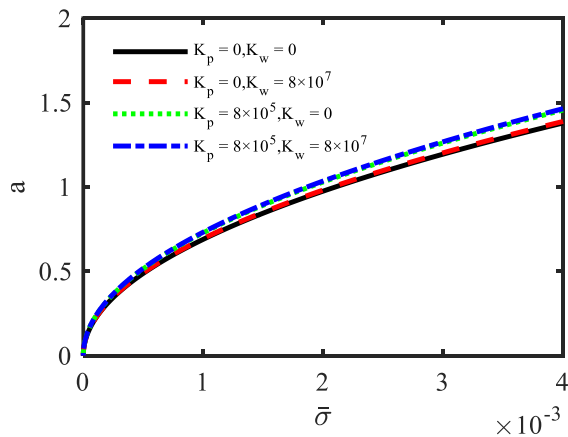


Fig. 14. Effect of elastic foundation coefficients.

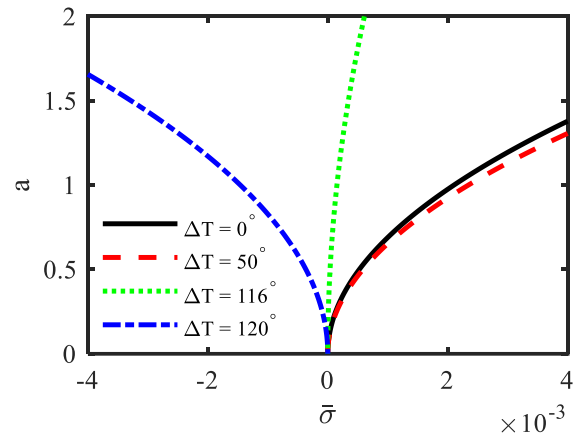


Fig. 15. Effect of porous type changes.

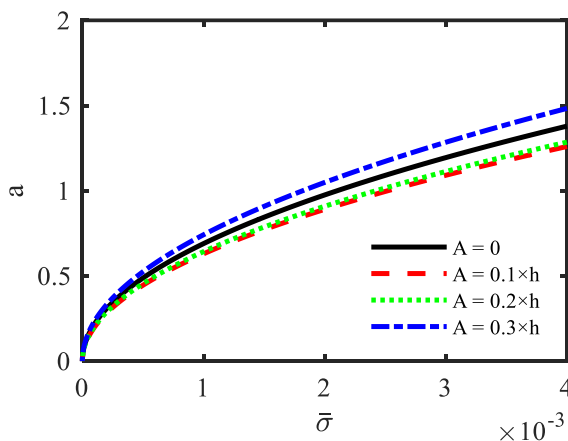
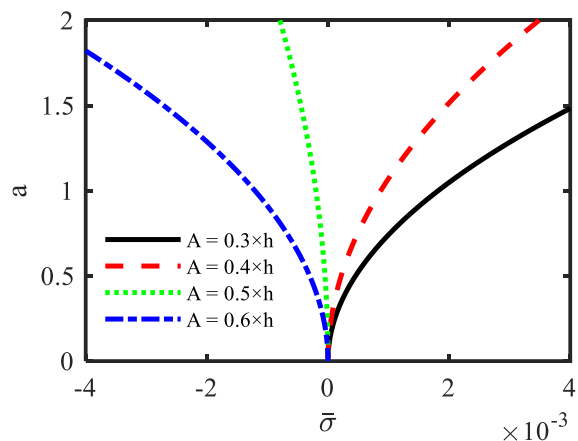


Fig. 16. Effect of imperfection amplitude changes.



OCPs were extracted, discretized, and converted into ODEs. Finally, by using the multiscale method, the relationship of nonlinear frequencies was extracted and the numerical results were validated with previous research. Then, the effect of changes in different geometric and material parameters was reported on the frequency response curve.

Some important results are reported below:

By increasing the semi-vertex angle parameter, the system behavior changes between the hardening and softening states.

The system behaviour is highly influenced by the subtended angle, and by changing this parameter, the behavior changes from hardening to softening.

The increase in volume fraction causes the hardening behavior to decrease.

Utilizing Type 1 and Type 4 causes a decrease in the hardening behavior instead of using Type 2 and Type 3

Increasing the thickness of porous material can reduce the hardening behavior.

The presence of stiffeners in the system reduces the hardening behavior; increasing the number of stiffeners causes an increase in the hardening behavior, and changing the cross-section of stiffeners can increase the hardening behavior.

The use of an elastic medium can decrease the hardening behavior.

An increase in temperature causes the system's behaviour to change from hardening to softening.

Increasing the imperfection amplitude causes the system behaviour to change from hardening to softening.

Disclosure Statement:

The authors report there are no competing interests to declare.

References

- [1] A. Sofiyev, M. Avcar, P. Ozyigit, S. Adigozel, The free vibration of non-homogeneous truncated conical shells on a Winkler foundation, *International Journal of Engineering and Applied Sciences*, 1(1) (2009) 34-41.
- [2] M. Nekouei, M. Raghebi, M. Mohammadi, Free vibration analysis of laminated composite conical shells reinforced with shape memory alloy fibers, *Acta Mechanica*, 230 (2019) 4235-4255.
- [3] S. Javed, F. Al Mukahal, M. Salama, Free vibration analysis of composite conical shells with variable thickness, *Shock and Vibration*, 2020 (2020) 1-15.
- [4] A. Shekari, F.A. Ghasemi, K. Malekzadehfard, Free damped vibration of rotating truncated conical sandwich shells using an improved high-order theory, *Latin American Journal of Solids and Structures*, 14 (2017) 2291-2323.
- [5] L. Tong, Free vibration of composite laminated conical shells, *International Journal of Mechanical Sciences*, 35(1) (1993) 47-61.
- [6] S. Guo, P. Hu, S. Li, Free vibration analysis of composite conical shells using Walsh series method, *Materials Research Express*, 8(7) (2021) 075303.
- [7] L. Tong, Free vibration of orthotropic conical shells, *International Journal of Engineering Science*, 31(5) (1993) 719-733.
- [8] S. Wu, Y. Qu, H. Hua, Free vibration of laminated orthotropic conical shell on Pasternak foundation by a domain decomposition method, *Journal of Composite Materials*, 49(1) (2015) 35-52.
- [9] H. Amirabadi, F. Farhatnia, S.A. Eftekhari, R. Hosseini-Ara, Free vibration analysis of rotating functionally graded GPL-reinforced truncated thick conical shells under different boundary conditions, *Mechanics Based Design of Structures and Machines*, 50(11) (2022) 3821-3852.
- [10] L. Monterrubio, Free vibration of shallow shells using the Rayleigh—Ritz method and penalty parameters, *Proceedings of the Institution of Mechanical Engineers, Part C: Journal of Mechanical Engineering Science*, 223(10) (2009) 2263-2272.
- [11] H. Matsunaga, Free vibration and stability of functionally graded shallow shells according to a 2D higher-order deformation theory, *Composite Structures*, 84(2) (2008) 132-146.
- [12] N. Bardell, J. Dunsdon, R. Langley, Free vibration of thin, isotropic, open, conical panels, *Journal of Sound and Vibration*, 217(2) (1998) 297-320.
- [13] M. Akbari, Y. Kiani, M. Aghdam, M. Eslami, Free vibration of FGM Lévy conical panels, *Composite Structures*, 116 (2014) 732-746.
- [14] X. Zhao, K.M. Liew, Free vibration analysis of functionally graded conical shell panels by a meshless method, *Composite Structures*, 93(2) (2011) 649-664.
- [15] Y. Kiani, R. Dimitri, F. Tornabene, Free vibration study of composite conical panels reinforced with FG-CNTs, *Engineering Structures*, 172 (2018) 472-482.
- [16] P. Xiang, Q. Xia, L. Jiang, L. Peng, J. Yan, X. Liu, Free vibration analysis of FG-CNTRC conical shell panels using the kernel particle Ritz element-free method, *Composite Structures*, 255 (2021) 112987.
- [17] J. Zhao, G. Fan, J. Guan, H. Li, J. Liu, Z. Xie, P.K. Wong, Free vibration and dynamic analysis on free-constrained layer of graphene based on composite conical shell via Jacobi-Ritz method, *International Journal of Structural Stability and Dynamics*, (2023).
- [18] Z. Wang, S. Yang, Y. Hao, W. Zhang, W. Ma, X. Zhang, Modeling and Free Vibration Analysis of Variable Stiffness System for Sandwich Conical Shell Structures with Variable Thickness, *International Journal of Structural Stability and Dynamics*, (2023) 2350171.
- [19] K. Draiche, A. Tounsi, K.D. Ibrahim, Y. Tlidji, An improved mathematical model for static and dynamic analysis of functionally graded doubly-curved shells, *Archive of Applied Mechanics*, 94(6) (2024) 1589-1611.
- [20] C. Mei, K. Decha-Umphai, A finite element method for nonlinear forced vibrations of rectangular plates, *AIAA journal*, 23(7) (1985) 1104-1110.
- [21] P. Ribeiro, Forced large amplitude periodic vibrations of cylindrical shallow shells, *Finite Elements in Analysis and Design*, 44(11) (2008) 657-674.
- [22] D. Chakravorty, P. Sinha, J. Bandyopadhyay, Applications of FEM on free and forced vibration of laminated shells, *Journal of Engineering Mechanics*, 124(1) (1998) 1-8.
- [23] Z. Lei, L. Tong, Semi-analytical solutions of free and force vibration behaviors of GRC-FG cylindrical shells, *Steel and Composite Structures, An International Journal*, 32(5) (2019) 687-699.
- [24] G. Zhang, T. Li, X. Zhu, J. Yang, Y. Miao, Free and forced vibration characteristics of submerged finite elliptic cylindrical shell, *Ocean Engineering*, 129 (2017) 92-106.
- [25] Y. Qu, Y. Chen, X. Long, H. Hua, G. Meng, Free and forced vibration analysis of uniform and stepped circular cylindrical shells using a domain decomposition method, *Applied Acoustics*, 74(3) (2013) 425-439.
- [26] F.-M. Li, K. Kishimoto, W.-H. Huang, The calculations of natural frequencies and forced vibration responses of conical shell using the Rayleigh—Ritz method, *Mechanics Research Communications*, 36(5) (2009) 595-602.
- [27] X. Ma, G. Jin, Y. Xiong, Z. Liu, Free and forced vibration analysis of coupled conical—cylindrical shells with arbitrary boundary conditions, *International Journal of Mechanical Sciences*, 88 (2014) 122-137.
- [28] M. Chen, K. Xie, W. Jia, K. Xu, Free and forced vibration of ring-stiffened conical—cylindrical shells with arbitrary boundary conditions, *Ocean Engineering*, 108

- (2015) 241-256.
- [29] S.M. Zaidan, H.M. Hasan, Influences of angular velocity and periodic axial load on the dynamic instability of functionally graded porous cylindrical panels, *Archive of Applied Mechanics*, 93(7) (2023) 2793-2812.
- [30] A.H. Sofiyev, Modeling and solution of eigenvalue problems of laminated cylindrical shells consisting of nanocomposite plies in thermal environments, *Archive of Applied Mechanics*, 94(10) (2024) 3071-3099.
- [31] S.H. Arshad, M.N. Naeem, N. Sultana, A.G. Shah, Z. Iqbal, Vibration analysis of bi-layered FGM cylindrical shells, *Archive of Applied Mechanics*, 81 (2011) 319-343.
- [32] J. Woo, S. Meguid, L. Ong, Nonlinear free vibration behavior of functionally graded plates, *Journal of sound and vibration*, 289(3) (2006) 595-611.
- [33] N. Nanda, J. Bandyopadhyay, Nonlinear free vibration analysis of laminated composite cylindrical shells with cutouts, *Journal of reinforced Plastics and Composites*, 26(14) (2007) 1413-1427.
- [34] V.K. Singh, S.K. Panda, Nonlinear free vibration analysis of single/doubly curved composite shallow shell panels, *Thin-Walled Structures*, 85 (2014) 341-349.
- [35] T. Ueda, Non-linear free vibrations of conical shells, *Journal of Sound and Vibration*, 64(1) (1979) 85-95.
- [36] M.Y.A. Jamalabadi, P. Borji, M. Habibi, R. Pelalak, Nonlinear vibration analysis of functionally graded GPL-RC conical panels resting on elastic medium, *Thin-Walled Structures*, 160 (2021) 107370.
- [37] S. Yang, Y. Hao, W. Zhang, S. Li, Nonlinear dynamic behavior of functionally graded truncated conical shell under complex loads, *International Journal of Bifurcation and Chaos*, 25(02) (2015) 1550025.
- [38] L.K. Hoa, N.-T. Trung, P.V. Hoan, P.L. Ben, Nonlinear instability analysis of functionally graded sandwich truncated conical shells reinforced by stiffeners resting on elastic foundations, *International Journal of Structural Stability and Dynamics*, 19(08) (2019) 1950082.
- [39] Y. Niu, Y. Hao, M. Yao, W. Zhang, S. Yang, Nonlinear dynamics of imperfect FGM conical panel, *Shock and Vibration*, 2018 (2018).
- [40] V. Fakhari, A. Ohadi, Nonlinear vibration control of functionally graded plate with piezoelectric layers in thermal environment, *Journal of Vibration and Control*, 17(3) (2011) 449-469.
- [41] M. Talebitooti, K. Daneshjou, R. Talebitooti, Vibration and critical speed of orthogonally stiffened rotating FG cylindrical shell under thermo-mechanical loads using differential quadrature method, *Journal of Thermal Stresses*, 36(2) (2013) 160-188.
- [42] K. Gao, W. Gao, B. Wu, D. Wu, C. Song, Nonlinear primary resonance of functionally graded porous cylindrical shells using the method of multiple scales, *Thin-Walled Structures*, 125 (2018) 281-293.
- [43] D.Q. Chan, V.T.T. Anh, N.D. Duc, Vibration and nonlinear dynamic response of eccentrically stiffened functionally graded composite truncated conical shells surrounded by an elastic medium in thermal environments, *Acta Mechanica*, 230(1) (2019) 157-178.
- [44] N.D. Duc, K. Seung-Eock, D.Q. Chan, Thermal buckling analysis of FGM sandwich truncated conical shells reinforced by FGM stiffeners resting on elastic foundations using FSDT, *Journal of Thermal Stresses*, 41(3) (2018) 331-365.
- [45] S.S. Mirjavadi, M. Forsat, M.R. Barati, A.S. Hamouda, Analysis of nonlinear vibrations of CNT-/fiberglass-reinforced multi-scale truncated conical shell segments, *Mechanics Based Design of Structures and Machines*, 50(6) (2022) 2067-2083.
- [46] V. Eslamdoust, H. Ahmadi, H. Aris, Non-linear primary resonance analysis of stiffened FGM conical panels resting on viscoelastic foundation, *Mechanics Based Design of Structures and Machines*, 52(12) (2024) 10488-10515.
- [47] A.H. Nayfeh, D.T. Mook, *Nonlinear oscillations*, John Wiley & Sons, 2008.
- [48] Y. Hao, Y. Niu, W. Zhang, M. Yao, S. Li, Nonlinear vibrations of FGM circular conical panel under in-plane and transverse excitation, *Journal of Vibration Engineering & Technologies*, 6(6) (2018) 453-469.
- [49] H. Aris, H. Ahmadi, Using the higher-order shear deformation theory to analyze the free vibration of stiffened rotating FGM conical shells in a thermal environment, *Thin-Walled Structures*, 183 (2023) 110366.
- [50] K.M. Liew, T.Y. Ng, X. Zhao, Free vibration analysis of conical shells via the element-free kp-Ritz method, *Journal of Sound and Vibration*, 281(3-5) (2005) 627-645.
- [51] T. Irie, G. Yamada, K. Tanaka, Natural frequencies of truncated conical shells, *Journal of Sound and Vibration*, 92(3) (1984) 447-453.
- [52] C. Shu, An efficient approach for free vibration analysis of conical shells, *International Journal of Mechanical Sciences*, 38(8-9) (1996) 935-949.
- [53] R.B. Bhat, Natural frequencies of rectangular plates using characteristic orthogonal polynomials in Rayleigh-Ritz method, *Journal of sound and vibration*, 102(4) (1985) 493-499.
- [54] M.W. Teng, Y.Q. Wang, Nonlinear free vibration of rectangular plates reinforced with 3D graphene foam: Approximate analytical solution, *Results in Physics*, 17 (2020) 103147.
- [55] G. Singh, K.K. Raju, G.V. Rao, N. Iyengar, Non-linear vibrations of simply supported rectangular cross-ply plates, *Journal of Sound and Vibration*, 142(2) (1990) 213-226.
- [56] M. Sathyamoorthy, Effects of large amplitude, shear

and rotatory inertia on vibration of rectangular plates,
 Journal of Sound and Vibration, 63(2) (1979) 161-167.
 [57] C.-S. Chen, W.-S. Cheng, R.-D. Chien, J.-L. Doong,

Large amplitude vibration of an initially stressed cross
 ply laminated plates, Applied Acoustics, 63(9) (2002)
 939-956.

Appendix A

The constant coefficients L_{ijk} for Eqs. (44) and (45).

$$L_{101} = \frac{((L^1_{101} + L^2_{101}) \sin \delta + 2(L^3_{101} + L^4_{101}))(n\pi - \cos n\pi \sin n\pi) \bar{h}^{-2}}{8\bar{I}_0 n \pi \theta_0}$$

$$L^1_{101} = \frac{-1}{2} ((\pi^2 m^2 + 1) \bar{A}_{10}^{-N_x} + 2\bar{A}_{10}^{-N_\theta} - 2\bar{A}_{20}^{-N_x} + 2\bar{A}_{10}^{-N_\theta}) \theta_0^2 \cos^2 \delta$$

$$L^2_{101} = (3\bar{A}_{10}^{-N_x} \pi^2 \bar{R}_1^2 m^2 + (\frac{1}{2} \pi^2 m^2 + \frac{1}{2}) \bar{A}_{10}^{-N_x} + \bar{A}_{10}^{-N_\theta} - \bar{A}_{20}^{-N_x} + \bar{A}_{20}^{-N_\theta}) \theta_0^2 + \bar{A}_{60}^{-x\theta} \pi^2 n^2$$

$$L^3_{101} = -((\pi^2 m^2 + \frac{1}{2}) \bar{A}_{10}^{-N_x} + \bar{A}_{10}^{-N_\theta} - \bar{A}_{20}^{-N_x} + \bar{A}_{20}^{-N_\theta}) \theta_0^2 \cos^2 \delta$$

$$L^4_{101} = ((\bar{A}_{10}^{-N_x} \pi^2 \bar{R}_1^2 m^2 + (\pi^2 m^2 + \frac{1}{2}) \bar{A}_{10}^{-N_x} + \bar{A}_{10}^{-N_\theta} - \bar{A}_{20}^{-N_x} + \bar{A}_{20}^{-N_\theta}) \theta_0^2 + \bar{A}_{60}^{-N_x\theta} \pi^2 n^2) \bar{R}_1$$

$$L_{102} = -\frac{(L^1_{102} + L^2_{102})(n\pi - \cos n\pi \sin n\pi) \bar{h}^{-2}}{8\bar{I}_0 m \pi}$$

$$L^1_{102} = (\frac{2}{3} m^2 (\bar{A}_{60}^{-N_x\theta} + \bar{A}_{20}^{-N_x}) \pi^2 + \bar{A}_{10}^{-N_\theta} + \bar{A}_{10}^{-N_x} + 2\bar{A}_{60}^{-N_x\theta}) \cos \delta^2$$

$$L^2_{102} = \pi^2 \bar{h} m^2 (\sin \delta + 2\bar{R}_1) (\bar{A}_{61}^{-N_x\theta} + \bar{A}_{21}^{-N_x}) \cos \delta - 2\pi^2 m^2 \bar{R}_1^2 (\bar{A}_{60}^{-N_x\theta} + \bar{A}_{20}^{-N_x}) \sin \delta$$

$$- 2(\bar{A}_{60}^{-N_x\theta} + \bar{A}_{20}^{-N_x}) m^2 (\bar{R}_1^2 + \frac{1}{3}) \pi^2 - \bar{A}_{10}^{-N_\theta} - \bar{A}_{20}^{-N_x} - 2\bar{A}_{60}^{-N_x\theta}$$

$$L_{103} = \frac{2}{3} \frac{h^2}{\bar{I}_0 n \pi^2 m \theta_0} (\frac{7}{6} \theta_0^2 (\sin \delta + \bar{R}_1) (\bar{A}_{10}^{-N_x} + \bar{A}_{20}^{-N_\theta}) \cos^2 \delta (\frac{3}{2} \bar{A}_{10}^{-N_x} m^2 (\bar{R}_1^2 + \frac{1}{3}) \theta_0^2$$

$$+ (\frac{1}{2} \bar{A}_{20}^{-N_x} + \bar{A}_{60}^{-N_x\theta}) n^2) \sin \delta \pi^2 (-1)^{1+m} + (\frac{1}{2} \bar{A}_{10}^{-N_x} m^2 (\bar{R}_1^2 + 3) \theta_0^2 +$$

$$(\frac{1}{2} \bar{A}_{20}^{-N_x} + \bar{A}_{60}^{-N_x\theta}) n^2) \bar{R}_1 \pi^2 (-1)^{1+m} + \frac{1}{2} \theta_0^2 (\bar{A}_{10}^{-N_x} \pi^2 m^2 (\sin \delta + 3\bar{R}_1) \cos^2 \delta$$

$$+ \frac{7}{3} (\sin \delta + \bar{R}_1) (\bar{A}_{10}^{-N_x} + \bar{A}_{20}^{-N_\theta})) (-1)^m + \bar{R}_1 (\frac{7}{6} \theta_0^2 (\bar{A}_{10}^{-N_x} + \bar{A}_{20}^{-N_\theta}) \cos^2 \delta$$

$$- \frac{7}{6} \theta_0^2 (\bar{A}_{10}^{-N_x} + \bar{A}_{20}^{-N_\theta})) \cos^3 (n\pi) + \bar{R}_1 ((\frac{1}{2} \theta_0^2 m^2 \bar{A}_{10}^{-N_x} \bar{R}_1^2 + (\frac{1}{2} \bar{A}_{20}^{-N_\theta} + \bar{A}_{60}^{-N_x\theta}) n^2) \pi^2) \cos^3 (n\pi)$$

$$+ \frac{3}{16} \theta_0^2 (\frac{2}{3} \bar{A}_{20}^{-N_x} \pi^2 m^2 + \bar{A}_{10}^{-N_\theta} + \bar{A}_{20}^{-N_x}) \cos^3 \delta \sin(n\pi) - \frac{3}{32} \theta_0^2 \bar{h} m^2 \pi^2 ((\bar{A}_{11}^{-N_x} \pi^2 m^2 + \bar{A}_{11}^{-N_x}$$

$$+ 2\bar{A}_{11}^{-N_\theta} - 2\bar{A}_{21}^{-N_x} + 2\bar{A}_{21}^{-N_\theta}) \sin \delta) \cos^2 \delta \sin(n\pi) - \frac{3}{32} \theta_0^2 \bar{h} m^2 \pi^2 (4\bar{R}_1 (\bar{A}_{11}^{-N_x} \pi^2 m^2 + \frac{1}{2} \bar{A}_{11}^{-N_x}$$

$$+ \bar{A}_{11}^{-N_\theta} - \bar{A}_{21}^{-N_x} + \bar{A}_{21}^{-N_\theta})) \cos^2 \delta \sin(n\pi) - \frac{3}{16} \theta_0^2 \cos \delta (2\bar{A}_{20}^{-N_x} \sin \delta \bar{R}_1 m^2 \pi^2$$

$$+ 2(\bar{R}_1^2 + \frac{1}{3}) m^2 \bar{A}_{20}^{-N_x} \pi^2 + \bar{A}_{10}^{-N_\theta} + \bar{A}_{20}^{-N_x}) \sin(n\pi)$$

$$\begin{aligned}
 & + \frac{3}{8} \bar{h} m^2 \pi^2 \left(\left(\frac{3}{2} \bar{A}_{11}^{-N_x} \theta_0^2 (\bar{R}_1^2 + \frac{1}{6}) m^2 + n^2 (\bar{A}_{61}^{-N_{x\theta}} + \frac{1}{2} \bar{A}_{21}^{-N_x}) \right) \pi^2 \right) (\sin \delta + 2\bar{R}_1) \sin(n\pi) \\
 & + \frac{3}{8} \bar{h} m^2 \pi^2 \left(\frac{1}{4} \theta_0^2 (\bar{A}_{11}^{-N_x} + \bar{A}_{11}^{-N_\theta} - 2\bar{A}_{21}^{-N_x} + 2\bar{A}_{21}^{-N_\theta}) \right) (\sin \delta + 2\bar{R}_1) \sin(n\pi) \\
 & + \frac{1}{3} \left(\left(\frac{14}{3} \theta_0^2 (\sin \delta + \bar{R}_1) (\bar{A}_{10}^{-N_x} + \bar{A}_{20}^{-N_\theta}) \cos^2 \delta + (6\bar{A}_{10}^{-N_x} m^2 (\bar{R}_1^2 + \frac{1}{3}) \theta_0^2 + n^2 \bar{A}_{60}^{-N_{x\theta}}) \sin \delta \right) \bar{h} m \bar{A} (-1)^{1+m} \right) \\
 & + \frac{1}{3} \left((\bar{R}_1 (2\bar{A}_{10}^{-N_x} m^2 (\bar{R}_1^2 + 3) \theta_0^2 + n^2 \bar{A}_{60}^{-N_{x\theta}}) \pi^2) \bar{h} m \bar{A} (-1)^{1+m} \right)
 \end{aligned}$$

$$\begin{aligned}
 L_{104} = & \left(\frac{7}{3} \theta_0^2 (\bar{A}_{10}^{-N_x} + \bar{A}_{20}^{-N_\theta}) \cos^2 \delta + \pi^2 (3\bar{A}_{10}^{-N_x} m^2 (\bar{R}_1^2 + \frac{1}{3}) \theta_0^2 + n^2 (\bar{A}_{10}^{-N_x} + 2\bar{A}_{60}^{-N_{x\theta}})) \right) \sin \delta + \\
 & \left(\frac{7}{3} \theta_0^2 (\bar{A}_{10}^{-N_x} + \bar{A}_{20}^{-N_\theta}) \cos^2 \delta + \pi^2 (\bar{A}_{10}^{-N_x} m^2 (\bar{R}_1^2 + 3) \theta_0^2 + n^2 (\bar{A}_{20}^{-N_x} + 2\bar{A}_{60}^{-N_{x\theta}})) \right) \bar{R}_1 (-1)^{1+m} + \\
 & \left(\left(\frac{7}{3} \bar{A}_{20}^{-N_\theta} + \frac{7}{3} \bar{A}_{10}^{-N_x} + \bar{A}_{10}^{-N_x} \pi^2 \cos^2 \delta m^2 \right) \sin \delta + 3\bar{R}_1 (\bar{A}_{10}^{-N_x} \pi^2 \cos^2 \delta m^2 + \frac{7\bar{A}_{10}^{-N_x}}{9} + \frac{7\bar{A}_{20}^{-N_\theta}}{9}) \theta_0^2 (-1)^m + \right. \\
 & \left. \left(\frac{7}{3} \theta_0^2 (\bar{A}_{10}^{-N_x} + \bar{A}_{20}^{-N_\theta}) \cos^2 \delta + \left(-\frac{7}{3} \bar{A}_{10}^{-N_x} - \frac{7}{3} \bar{A}_{20}^{-N_\theta} + \bar{A}_{10}^{-N_x} \pi^2 \bar{R}_1 m^2 \right) \theta_0^2 + \pi^2 n^2 (\bar{A}_{20}^{-N_x} + 2\bar{A}_{60}^{-N_{x\theta}}) \right) \bar{R}_1 \cos^3 n\pi + \right. \\
 & \left. 3 \left(\left(\frac{7}{3} \bar{A}_{20}^{-N_\theta} + \frac{7}{3} \bar{A}_{10}^{-N_x} + \bar{A}_{10}^{-N_x} \pi^2 \cos^2 \delta m^2 \right) \sin \delta + 3\bar{R}_1 (\bar{A}_{10}^{-N_x} \pi^2 \cos^2 \delta m^2 + \frac{7\bar{A}_{10}^{-N_x}}{9} + \frac{7\bar{A}_{20}^{-N_\theta}}{9}) \theta_0^2 (-1)^{1+m} + \right. \right. \\
 & \left. \left. (7\theta_0^2 (\bar{A}_{10}^{-N_x} + \bar{A}_{20}^{-N_\theta}) \cos^2 \delta + 3(3\bar{A}_{10}^{-N_x} m^2 (\bar{R}_1^2 + \frac{1}{3}) \theta_0^2 + n^2 \bar{A}_{60}^{-N_{x\theta}}) \pi^2) \sin \delta + 3\bar{R}_1 \left(\frac{7}{3} \theta_0^2 (\bar{A}_{10}^{-N_x} + \bar{A}_{20}^{-N_\theta}) \cos^2 \delta + \right. \right. \right. \\
 & \left. \left. \left. + (\bar{A}_{10}^{-N_x} m^2 (\bar{R}_1^2 + 3) \theta_0^2 + n^2 \bar{A}_{60}^{-N_{x\theta}}) \pi^2 \right) (-1)^m \right. \right. \\
 & \left. \left. - 3 \left(\frac{7}{3} \theta_0^2 (\bar{A}_{10}^{-N_x} + \bar{A}_{20}^{-N_\theta}) \cos^2 \delta + \left(-\frac{7}{3} \bar{A}_{10}^{-N_x} - \frac{7}{3} \bar{A}_{20}^{-N_\theta} + \bar{A}_{10}^{-N_x} \pi^2 \bar{R}_1 m^2 \right) \theta_0^2 + \bar{A}_{60}^{-N_{x\theta}} \pi^2 n^2 \right) \bar{R}_1 \cos n\pi + \right. \right. \\
 & \left. \left. \left(\frac{14}{3} \theta_0^2 (\bar{A}_{10}^{-N_x} + \bar{A}_{20}^{-N_\theta}) \cos^2 \delta + \pi^2 (6\bar{A}_{10}^{-N_x} m^2 (\bar{R}_1^2 + \frac{1}{3}) \theta_0^2 + n^2 \bar{A}_{60}^{-N_{x\theta}}) \right) \sin \delta + \right. \right. \\
 & \left. \left. \left(\frac{14}{3} \theta_0^2 (\bar{A}_{10}^{-N_x} + \bar{A}_{20}^{-N_\theta}) \cos^2 \delta + \pi^2 (2\bar{A}_{10}^{-N_x} m^2 (\bar{R}_1^2 + 3) \theta_0^2 + n^2 \bar{A}_{60}^{-N_{x\theta}}) \right) \bar{R}_1 (-1)^{1+m} + \right. \right. \\
 & \left. \left. (2\bar{A}_{10}^{-N_x} \pi^2 \cos^2 \delta m^2 \theta_0^2 + \frac{14}{3} \theta_0^2 (\bar{A}_{10}^{-N_x} + \bar{A}_{20}^{-N_\theta}) + \bar{A}_{20}^{-N_x} \pi^2 n^2) \sin \delta + \right. \right. \\
 & \left. \left. + \bar{R}_1 (6\bar{A}_{10}^{-N_x} \pi^2 \cos^2 \delta m^2 \theta_0^2 + \frac{14}{3} \theta_0^2 (\bar{A}_{10}^{-N_x} + \bar{A}_{20}^{-N_\theta}) + \bar{A}_{20}^{-N_x} \pi^2 n^2) (-1)^{1+m} + \right. \right. \\
 & \left. \left. - \bar{R}_1 \left(-\frac{14}{3} \theta_0^2 (\bar{A}_{10}^{-N_x} + \bar{A}_{20}^{-N_\theta}) \cos^2 \delta + (-2\bar{A}_{10}^{-N_x} \pi^2 \bar{R}_1 m^2 + \frac{14}{3} (\bar{A}_{10}^{-N_x} + \bar{A}_{20}^{-N_\theta})) \theta_0^2 + \pi^2 n^2 (\bar{A}_{10}^{-N_x} - \bar{A}_{60}^{-N_{x\theta}}) \right) \right. \right.
 \end{aligned}$$

$$L_{105} = \frac{L_{105}^1 (n\pi - \cos n\pi \sin n\pi) \theta_0}{4n\pi^3 m^2}$$

$$\begin{aligned}
 L_{105}^1 = & \left(\left(-\frac{1}{4} \pi^2 m^2 - \frac{3}{4} \right) \cos^2 \delta + \frac{3}{4} + \frac{3}{2} (\bar{R}_1^2 + \frac{1}{6}) m^2 \pi^2 \right) \sin(\delta) \\
 & + \bar{R}_1 \left(\left(-\pi^2 m^2 - \frac{3}{2} \right) \cos^2 \delta + \frac{3}{2} + m^2 (\bar{R}_1^2 + 1) \pi^2 \right)
 \end{aligned}$$

$$\begin{aligned}
 & + \frac{3}{8} \bar{h} m^2 \pi^2 \left(\left(\frac{3}{2} \bar{A}_{11}^{N_x} \theta_0^2 (\bar{R}_1^2 + \frac{1}{6}) m^2 + n^2 (\bar{A}_{61}^{N_{x\theta}} + \frac{1}{2} \bar{A}_{21}^{N_x}) \right) \pi^2 (\sin \delta + 2\bar{R}_1) \sin(n\pi) \right. \\
 & + \frac{3}{8} \bar{h} m^2 \pi^2 \left(\frac{1}{4} \theta_0^2 (\bar{A}_{11}^{N_x} + \bar{A}_{11}^{N_\theta} - 2\bar{A}_{21}^{N_x} + 2\bar{A}_{21}^{N_\theta}) \right) (\sin \delta + 2\bar{R}_1) \sin(n\pi) \\
 & + \frac{1}{3} \left(\left(\frac{14}{3} \theta_0^2 (\sin \delta + \bar{R}_1) (\bar{A}_{10}^{N_x} + \bar{A}_{20}^{N_\theta}) \cos^2 \delta + (6\bar{A}_{10}^{N_x} m^2 (\bar{R}_1^2 + \frac{1}{3}) \theta_0^2 + n^2 \bar{A}_{60}^{N_{x\theta}}) \sin \delta \right) \bar{h} m \bar{A} (-1)^{1+m} \right) \\
 & + \frac{1}{3} \left((\bar{R}_1 (2\bar{A}_{10}^{N_x} m^2 (\bar{R}_1^2 + 3) \theta_0^2 + n^2 \bar{A}_{60}^{N_{x\theta}}) \pi^2) \bar{h} m \bar{A} (-1)^{1+m} \right)
 \end{aligned}$$

$$\begin{aligned}
 L_{104} & = \left(\frac{7}{3} \theta_0^2 (\bar{A}_{10}^{N_x} + \bar{A}_{20}^{N_\theta}) \cos^2 \delta + \pi^2 (3\bar{A}_{10}^{N_x} m^2 (\bar{R}_1^2 + \frac{1}{3}) \theta_0^2 + n^2 (\bar{A}_{10}^{N_x} + 2\bar{A}_{60}^{N_{x\theta}})) \right) \sin \delta + \\
 & \left(\frac{7}{3} \theta_0^2 (\bar{A}_{10}^{N_x} + \bar{A}_{20}^{N_\theta}) \cos^2 \delta + \pi^2 (\bar{A}_{10}^{N_x} m^2 (\bar{R}_1^2 + 3) \theta_0^2 + n^2 (\bar{A}_{20}^{N_x} + 2\bar{A}_{60}^{N_{x\theta}})) \right) \bar{R}_1 (-1)^{1+m} + \\
 & \left(\left(\frac{7}{3} \bar{A}_{20}^{N_\theta} + \frac{7}{3} \bar{A}_{10}^{N_x} + \bar{A}_{10}^{N_x} \pi^2 \cos^2 \delta m^2 \right) \sin \delta + 3\bar{R}_1 (\bar{A}_{10}^{N_x} \pi^2 \cos^2 \delta m^2 + \frac{7\bar{A}_{10}^{N_x}}{9} + \frac{7\bar{A}_{20}^{N_\theta}}{9}) \right) \theta_0^2 (-1)^m + \\
 & \left(\frac{7}{3} \theta_0^2 (\bar{A}_{10}^{N_x} + \bar{A}_{20}^{N_\theta}) \cos^2 \delta + \left(-\frac{7}{3} \bar{A}_{10}^{N_x} - \frac{7}{3} \bar{A}_{20}^{N_\theta} + \bar{A}_{10}^{N_x} \pi^2 \bar{R}_1 m^2 \right) \theta_0^2 + \pi^2 n^2 (\bar{A}_{20}^{N_x} + 2\bar{A}_{60}^{N_{x\theta}}) \right) \bar{R}_1 \cos^3 n\pi + \\
 & 3 \left(\frac{7}{3} \bar{A}_{20}^{N_\theta} + \frac{7}{3} \bar{A}_{10}^{N_x} + \bar{A}_{10}^{N_x} \pi^2 \cos^2 \delta m^2 \right) \sin \delta + 3\bar{R}_1 (\bar{A}_{10}^{N_x} \pi^2 \cos^2 \delta m^2 + \frac{7\bar{A}_{10}^{N_x}}{9} + \frac{7\bar{A}_{20}^{N_\theta}}{9}) \theta_0^2 (-1)^{1+m} + \\
 & (7\theta_0^2 (\bar{A}_{10}^{N_x} + \bar{A}_{20}^{N_\theta}) \cos^2 \delta + 3(3\bar{A}_{10}^{N_x} m^2 (\bar{R}_1^2 + \frac{1}{3}) \theta_0^2 + n^2 \bar{A}_{60}^{N_{x\theta}}) \pi^2) \sin \delta + 3\bar{R}_1 \left(\frac{7}{3} \theta_0^2 (\bar{A}_{10}^{N_x} + \bar{A}_{20}^{N_\theta}) \cos^2 \delta + \right. \\
 & \left. + (\bar{A}_{10}^{N_x} m^2 (\bar{R}_1^2 + 3) \theta_0^2 + n^2 \bar{A}_{60}^{N_{x\theta}}) \pi^2 \right) (-1)^m \\
 & - 3 \left(\frac{7}{3} \theta_0^2 (\bar{A}_{10}^{N_x} + \bar{A}_{20}^{N_\theta}) \cos^2 \delta + \left(-\frac{7}{3} \bar{A}_{10}^{N_x} - \frac{7}{3} \bar{A}_{20}^{N_\theta} + \bar{A}_{10}^{N_x} \pi^2 \bar{R}_1 m^2 \right) \theta_0^2 + \bar{A}_{60}^{N_{x\theta}} \pi^2 n^2 \right) \bar{R}_1 \cos n\pi +
 \end{aligned}$$

$$L_{202} = \frac{1}{4} (n\pi + \cos n\pi \sin n\pi) n \frac{(L_{202}^1 + L_{202}^2)}{\theta_0 \pi^3 m^4}$$

$$\begin{aligned}
 L_{202}^1 & = \left(\frac{1}{5} m^4 \pi^4 - \pi^2 m^2 + \frac{3}{2} \right) \cos^4 \delta + (-\pi^2 \bar{R}_1 m^2 (\pi^2 m^2 - 3) \sin \delta - 3 \\
 & - 2(\bar{R}_1^2 + \frac{1}{5}) m^4 \pi^4 + m^2 (3\bar{R}_1^2 + 2) \pi^2) \cos^2 \delta
 \end{aligned}$$

$$L_{202}^2 = 2 \left(-\frac{3}{2} + m^2 (\bar{R}_1^2 + \frac{1}{2}) \pi^2 \right) \pi^2 \bar{R}_1 m^2 \sin \delta + \frac{3}{2} + m^4 (\bar{R}_1^4 + 2\bar{R}_1^2 + \frac{1}{5}) \pi^4 + (-3\bar{R}_1^2 - 1) m^2 \pi^2$$

$$\begin{aligned}
 L_{203}^1 & = \frac{4}{9} A m \bar{h} \left(\frac{13\theta_0^2 \cos^2 \delta}{9} \left(\frac{9\pi^2 m^2 \bar{A}_{21}^{M_\theta}}{26} + \bar{A}_{61}^{M_{x\theta}} \right) + \theta_0^2 \bar{A}_{61}^{M_{x\theta}} (\pi^2 m^2 \bar{R}_1 + \frac{1}{3} \sin \alpha) \sin \delta \right. \\
 & + \frac{1}{2} \bar{A}_{61}^{M_{x\theta}} \pi^2 \theta_0^2 (\bar{R}_1^2 + 1) m^2 + \bar{A}_{11}^{M_\theta} \pi^2 n^2 + \frac{7\bar{A}_{21}^{M_\theta} \theta_0^2}{9} \left. \right) \cos \alpha + \frac{3}{2} \theta_0^2 \left(\left(\frac{1}{3} \bar{A}_{60}^{N_{x\theta}} \pi^2 m^2 + \frac{14\bar{A}_{20}^{N_\theta}}{9} \right) \sin \delta \right. \\
 & + \frac{4}{9} \bar{A}_{60}^{N_{x\theta}} \sin \alpha + \frac{14\bar{R}_1}{9} \left(\frac{9\bar{A}_{60}^{N_{x\theta}} \pi^2 m^2}{14} + \bar{A}_{20}^{N_\theta} \right) \cos^2 \delta + \left. \left(m^2 \bar{A}_{20}^{N_\theta} (\bar{R}_1^2 + \frac{1}{3}) \pi^2 + \frac{26\bar{A}_{60}^{N_{x\theta}}}{9} \right) \sin \delta \right. \\
 & + \left. \frac{1}{3} \bar{R}_1 (m^2 \bar{A}_{20}^{N_\theta} (\bar{R}_1^2 + 3) \pi^2 + \frac{26\bar{A}_{60}^{N_{x\theta}}}{3}) \right) \bar{h} (-1)^{1+m+n}
 \end{aligned}$$

$$L^2_{203} = \frac{1}{2}Am(\theta_0^2((\pi^2 m^2 \bar{A}_{61}^{M_{x\theta}} + \frac{14\bar{A}_{21}^{M_\theta}}{9})\cos^2 \delta + 2\pi^2 m^2 \bar{A}_{21}^{M_\theta} \sin \delta \bar{R}_1 + m^2 \bar{A}_{21}^{M_\theta} (\bar{R}_1^2 + 1)\pi^2 + \frac{26\bar{A}_{61}^{M_{x\theta}}}{9})\bar{h} \cos \alpha + ((\pi^2 m^2 \bar{A}_{20}^{N_\theta} + \frac{26\bar{A}_{60}^{N_{x\theta}}}{3})\sin \delta + 3\bar{R}_1(\pi^2 m^2 \bar{A}_{20}^{N_\theta} + \frac{26\bar{A}_{60}^{N_{x\theta}}}{9}))\theta_0^2 \cos^2 \delta + (\frac{4}{3}\bar{A}_{60}^{N_{x\theta}} \sin \alpha \bar{R}_1 \theta_0^2 + 3\theta_0^2 \pi^2 (\bar{R}_1^2 + \frac{1}{3})\bar{A}_{60}^{N_{x\theta}} m^2 + 2\bar{A}_{10}^{N_\theta} \pi^2 n^2 + \frac{14}{3}\bar{A}_{20}^{N_\theta} \theta_0^2)\sin \delta + \frac{4}{3}\bar{A}_{60}^{N_{x\theta}} \sin \alpha \theta_0^2 + 2\bar{R}_1(\frac{1}{2}\bar{A}_{60}^{N_{x\theta}} \pi^2 \theta_0^2 (\bar{R}_1^2 + 3)m^2 + \bar{A}_{10}^{N_\theta} \pi^2 n^2 + \frac{7}{3}\bar{A}_{20}^{N_\theta} \theta_0^2))\bar{h}(-1)^{m+n}$$

$$L^3_{203} = \frac{1}{2}Am(\theta_0^2((\pi^2 m^2 \bar{A}_{61}^{M_{x\theta}} + \frac{14\bar{A}_{21}^{M_\theta}}{9})\cos^2 \delta + 2\pi^2 m^2 \bar{A}_{21}^{M_\theta} \sin \delta \bar{R}_1 + m^2 \bar{A}_{21}^{M_\theta} (\bar{R}_1^2 + 1)\pi^2 + \frac{26\bar{A}_{61}^{M_{x\theta}}}{9})\bar{h} \cos \alpha + ((\pi^2 m^2 \bar{A}_{20}^{N_\theta} + \frac{26\bar{A}_{60}^{N_{x\theta}}}{3})\sin \delta + 3\bar{R}_1(\pi^2 m^2 \bar{A}_{20}^{N_\theta} + \frac{26\bar{A}_{60}^{N_{x\theta}}}{9}))\theta_0^2 \cos^2 \delta + (\frac{4}{3}\bar{A}_{60}^{N_{x\theta}} \sin \alpha \bar{R}_1 \theta_0^2 + 3\theta_0^2 \pi^2 (\bar{R}_1^2 + \frac{1}{3})\bar{A}_{60}^{N_{x\theta}} m^2 + 2\bar{A}_{10}^{N_\theta} \pi^2 n^2 + \frac{14}{3}\bar{A}_{20}^{N_\theta} \theta_0^2)\sin \delta + \frac{4}{3}\bar{A}_{60}^{N_{x\theta}} \sin \alpha \theta_0^2 + 2\bar{R}_1(\frac{1}{2}\bar{A}_{60}^{N_{x\theta}} \pi^2 \theta_0^2 (\bar{R}_1^2 + 3)m^2 + \bar{A}_{10}^{N_\theta} \pi^2 n^2 + \frac{7}{3}\bar{A}_{20}^{N_\theta} \theta_0^2))\bar{h}(-1)^{1+n}$$

$$L^4_{203} = \frac{13Am\bar{h}(-1)^{1+n}}{9}(\bar{h}\theta_0^2(\frac{9\pi^2 m^2 \bar{A}_{21}^{M_\theta} \bar{R}_1^2}{26} + \frac{7\bar{A}_{21}^{M_\theta} \cos^2 \delta}{13} + \bar{A}_{61}^{M_{x\theta}})\cos \alpha + \frac{9\bar{R}_1}{13}(\frac{1}{2}\bar{A}_{60}^{N_{x\theta}} \pi^2 \bar{R}_1^2 m^2 \theta_0^2 + \bar{A}_{10}^{N_\theta} \pi^2 n^2 + \frac{13}{3}\bar{A}_{60}^{N_{x\theta}} \cos^2 \delta \theta_0^2 + \frac{2}{3}\bar{A}_{60}^{N_{x\theta}} \sin \alpha \theta_0^2 \sin(\delta) + \frac{7}{3}\bar{A}_{20}^{N_\theta} \theta_0^2))$$

$$L^5_{203} = -\frac{9}{4} \frac{L^1_{203}}{(-1)^n}$$

$$L^6_{203} = \frac{1}{2}Am(\bar{h}(\bar{A}_{61}^{M_{x\theta}} \pi^2 \bar{R}_1^2 m^2 \theta_0^2 + \frac{26}{9}\bar{A}_{61}^{M_{x\theta}} \cos^2 \delta \theta_0^2 + \frac{2}{3}\theta_0^2 \bar{A}_{61}^{M_{x\theta}} \sin \alpha \sin \delta + 2\bar{A}_{11}^{M_\theta} \pi^2 n^2 + \frac{14\bar{A}_{21}^{M_\theta} \theta_0^2}{9})\cos \alpha + \bar{R}_1 \theta_0^2 (\pi^2 m^2 \bar{A}_{20}^{N_\theta} \bar{R}_1^2 + \frac{14}{3}\bar{A}_{20}^{N_\theta} \cos^2 \delta + \frac{26\bar{A}_{60}^{N_{x\theta}}}{3}))\bar{h}(-1)^n$$

$$L^7_{203} = -\frac{1}{2}m\bar{h}(\frac{26}{9}\theta_0^2 \bar{h} \cos^2 \delta (\frac{1}{104}(27\bar{A}_{62}^{M_{x\theta}} + \frac{27}{2}\bar{A}_{22}^{M_\theta})\pi^4 nm^3 - \frac{1}{104}(81\bar{A}_{62}^{M_{x\theta}} - \frac{81}{4}\bar{A}_{12}^{M_\theta} + \frac{81}{4}\bar{A}_{22}^{M_\theta})\pi^2 nm + \bar{A}(\bar{A}_{61}^{M_{x\theta}} - \frac{7}{13}\bar{A}_{21}^{M_\theta})) + \frac{9\bar{A}_{11}^{M_\theta} \pi^2 mn \theta_0^2 (\sin \delta + 2\bar{R}_1) \cos \delta}{16} + \frac{2}{3}\theta_0^2 ((-\frac{27}{16}\bar{A}_{62}^{M_{x\theta}} \pi^2 mn + \bar{A}_{61}^{M_{x\theta}} \bar{A}) \sin \alpha - \frac{1}{8}(27\bar{A}_{62}^{M_{x\theta}} + \frac{27\bar{A}_{22}^{M_\theta}}{2})\pi^4 m^3 \bar{R}_1 n) \sin \delta - \frac{9}{4}(\bar{A}_{62}^{M_{x\theta}} + \frac{\bar{A}_{22}^{M_\theta}}{2})\theta_0^2 \pi^4 (\bar{R}_1^2 + \frac{1}{3})nm^3 + \bar{A} \pi^2 \bar{R}_1^2 \theta_0^2 (\bar{A}_{61}^{M_{x\theta}} - \bar{A}_{21}^{M_\theta})m^2 + \frac{9}{4}((\bar{A}_{62}^{M_{x\theta}} - \frac{\bar{A}_{12}^{M_\theta}}{4} + \frac{\bar{A}_{22}^{M_\theta}}{4})\theta_0^2 - \frac{1}{2}\bar{A}_{12}^{M_\theta} \pi^2 n^2)\pi^2 nm - \frac{26\bar{A}}{9}((\bar{A}_{61}^{M_{x\theta}} - \frac{7\bar{A}_{21}^{M_\theta}}{13})\theta_0^2 - \frac{9\bar{A}_{11}^{M_\theta} \pi^2 n^2}{13}))\cos \alpha$$

$$L_{203}^8 = -\frac{3}{16} \bar{A}_{10}^{-N_\theta} (\pi^2 m^2 - \frac{3}{2}) \theta_0^2 n \cos^3 \delta$$

$$L_{203}^9 = -\frac{7}{3} \theta_0^2 m (-\frac{27}{224} \pi^2 m (\pi^2 (\bar{A}_{61}^{-N_{x\theta}} + \frac{\bar{A}_{21}^{-N_\theta}}{2}) m^2 - 5 \bar{A}_{61}^{-N_{x\theta}} + \bar{A}_{11}^{-N_\theta} - \frac{3}{2} \bar{A}_{21}^{-N_\theta}) n \sin \delta - \frac{27}{112} \bar{A}_{61}^{-N_{x\theta}} \pi^2 \sin \alpha m n$$

$$+ (-\frac{1}{56} (27 \bar{A}_{61}^{-N_{x\theta}} + \frac{27}{2} \bar{A}_{21}^{-N_\theta}) \pi^4 n m^3 + \frac{1}{112} (135 \bar{A}_{61}^{-N_{x\theta}} - 27 \bar{A}_{11}^{-N_\theta} + \frac{81 \bar{A}_{21}^{-N_\theta}}{2}) \pi^2 n m + \bar{A} (\bar{A}_{20}^{-N_\theta} - \frac{13}{7} \bar{A}_{60}^{-N_{x\theta}})) R b 1) \bar{h} \cos^2 \delta$$

$$L_{203}^{10} = \frac{9}{16} \bar{A}_{10}^{-N_\theta} (\sin \delta \pi^2 \bar{R}_1 m^2 - \frac{1}{2} + \pi^2 (\bar{R}_1^2 + \frac{1}{3}) m^2) \theta_0^2 n \cos \delta m \bar{h}$$

$$L_{203} = \frac{\bar{h}^2}{I_0 \theta_0^2 \pi m^2} (L_{203}^1 + L_{203}^2 + L_{203}^3 + L_{203}^4 + L_{203}^5 + L_{203}^6 + L_{203}^7 + L_{203}^8 + L_{203}^9 + L_{203}^{10})$$

$$L_{204}^1 = (\bar{h} (\frac{1}{2} (\pi^2 m^2 \bar{A}_{21}^{-M_\theta} + \frac{26}{9} \bar{A}_{61}^{-M_{x\theta}}) \theta_0^2 \cos^2 \delta + \theta_0^2 \bar{A}_{61}^{-M_{x\theta}} (\pi^2 m^2 \bar{R}_1 + \frac{1}{3} \sin \alpha) \sin \delta$$

$$+ (\frac{1}{2} m^2 \bar{A}_{61}^{-M_{x\theta}} (\bar{R}_1^2 + 1) \pi^2 + \frac{7}{9} \bar{A}_{21}^{-M_\theta}) \theta_0^2 + \bar{A}_{11}^{-M_\theta} \pi^2 n^2) \cos \alpha + \frac{3}{2} ((\frac{1}{3} \pi^2 m^2 \bar{A}_{60}^{-N_{x\theta}} + \frac{14}{9} \bar{A}_{20}^{-N_\theta}) \sin \delta + \frac{4}{9} \bar{A}_{60}^{-N_{x\theta}} \sin \alpha + R b 1 (\pi^2 m^2 \bar{A}_{60}^{-N_{x\theta}} + \frac{14}{9} \bar{A}_{20}^{-N_\theta})) \cos^2 \delta + (m^2 \bar{A}_{20}^{-N_\theta} (\bar{R}_1^2 + \frac{1}{3}) \pi^2 + \frac{26}{9} \bar{A}_{60}^{-N_{x\theta}}) \sin \delta + \frac{1}{3} \bar{R}_1 (m^2 \bar{A}_{20}^{-N_\theta} (\bar{R}_1^2 + 3) \pi^2 + \frac{26}{3} \bar{A}_{60}^{-N_{x\theta}}) \theta_0^2) (-1)^{1+m+n}$$

$$L_{204}^2 = (((\frac{1}{2} \pi^2 m^2 \bar{A}_{61}^{-M_{x\theta}} + \frac{7 \bar{A}_{21}^{-M_\theta}}{9}) \cos^2 \delta + \pi^2 m^2 \bar{A}_{21}^{-M_\theta} \sin \delta \bar{R}_1 + \frac{1}{2} m^2 \bar{A}_{21}^{-M_\theta} (\bar{R}_1^2 + 1) \pi^2 + \frac{13 \bar{A}_{61}^{-M_{x\theta}}}{9}) \bar{h} \theta_0^2 \cos \alpha + \frac{1}{2} ((\pi^2 m^2 \bar{A}_{20}^{-N_\theta} + \frac{26}{3} \bar{A}_{60}^{-N_{x\theta}}) \sin \delta + 3 \bar{R}_1 (\pi^2 m^2 \bar{A}_{20}^{-N_\theta} + \frac{26 \bar{A}_{60}^{-N_{x\theta}}}{9})) \theta_0^2 \cos^2 \delta + (\frac{2}{3} \bar{A}_{60}^{-N_{x\theta}} \sin \alpha \bar{R}_1 \theta_0^2 + (\frac{3}{2} (\bar{R}_1^2 + \frac{1}{3}) \bar{A}_{60}^{-N_{x\theta}} m^2 \pi^2 + \frac{7}{3} \bar{A}_{20}^{-N_\theta}) \theta_0^2 + A b 10 N 2 \pi^2 n^2) \sin \delta + \frac{2}{3} \theta_0^2 \bar{A}_{60}^{-N_{x\theta}} \sin \alpha + \bar{R}_1 ((\frac{1}{2} \bar{A}_{60}^{-N_{x\theta}} m^2 (\bar{R}_1^2 + 3) \pi^2 + \frac{7}{3} \bar{A}_{20}^{-N_\theta}) \theta_0^2 + \bar{A}_{10}^{-N_\theta} \pi^2 n^2)) (-1)^{1+m+n}$$

$$L_{204}^3 = -(((\frac{1}{2} \pi^2 m^2 \bar{A}_{61}^{-M_{x\theta}} + \frac{7 \bar{A}_{21}^{-M_\theta}}{9}) \cos^2 \delta + \pi^2 m^2 \bar{A}_{21}^{-M_\theta} \sin \delta \bar{R}_1 + \frac{1}{2} m^2 \bar{A}_{21}^{-M_\theta} (\bar{R}_1^2 + 1) \pi^2 + \frac{13 \bar{A}_{61}^{-M_{x\theta}}}{9}) \bar{h} \theta_0^2 \cos \alpha + \frac{1}{2} ((\pi^2 m^2 \bar{A}_{20}^{-N_\theta} + \frac{26}{3} \bar{A}_{60}^{-N_{x\theta}}) \sin \delta + 3 \bar{R}_1 (\pi^2 m^2 \bar{A}_{20}^{-N_\theta} + \frac{26 \bar{A}_{60}^{-N_{x\theta}}}{9})) \theta_0^2 \cos^2 \delta + (\frac{2}{3} \bar{A}_{60}^{-N_{x\theta}} \sin \alpha \bar{R}_1 \theta_0^2 + (\frac{3}{2} (\bar{R}_1^2 + \frac{1}{3}) \bar{A}_{60}^{-N_{x\theta}} m^2 \pi^2 + \frac{7}{3} \bar{A}_{20}^{-N_\theta}) \theta_0^2 + \bar{A}_{10}^{-N_\theta} \pi^2 n^2) \sin \delta + \frac{2}{3} \theta_0^2 \bar{A}_{60}^{-N_{x\theta}} \sin \alpha + \bar{R}_1 ((\frac{1}{2} \bar{A}_{60}^{-N_{x\theta}} m^2 (\bar{R}_1^2 + 3) \pi^2 + \frac{7}{3} \bar{A}_{20}^{-N_\theta}) \theta_0^2 + \bar{A}_{10}^{-N_\theta} \pi^2 n^2)) (-1)^{2+m}$$

$$L_{204}^4 = (\frac{1}{2} \bar{h} \theta_0^2 (\pi^2 m^2 \bar{A}_{21}^{-M_\theta} \bar{R}_1^2 + \frac{14}{9} \bar{A}_{21}^{-M_\theta} \cos^2 \delta + \frac{26}{9} \bar{A}_{61}^{-M_{x\theta}}) \cos \alpha + \bar{R}_1 (\frac{13}{3} \bar{A}_{60}^{-N_{x\theta}} \theta_0^2 + \frac{2}{3} \theta_0^2 \bar{A}_{60}^{-N_{x\theta}} \sin \alpha \sin \delta + (\frac{7}{3} \bar{A}_{20}^{-N_\theta} + \frac{1}{2} \pi^2 m^2 \bar{A}_{60}^{-N_{x\theta}} \bar{R}_1^2) \theta_0^2 + \bar{A}_{10}^{-N_\theta} \pi^2 n^2)) (-1)^{1+n}$$

$$L_{204}^5 = (\bar{h} (\frac{1}{2} (\pi^2 m^2 \bar{A}_{21}^{-M_\theta} + \frac{26}{9} \bar{A}_{61}^{-M_{x\theta}}) \theta_0^2 \cos^2 \delta + \theta_0^2 \bar{A}_{61}^{-M_{x\theta}} (\pi^2 m^2 \bar{R}_1 + \frac{1}{3} \sin \alpha) \sin \delta + (\frac{1}{2} m^2 \bar{A}_{61}^{-M_{x\theta}} (\bar{R}_1^2 + 1) \pi^2$$

$$+ \frac{7\bar{A}_{21}^{M_\theta}}{9})\theta_0^2 + \bar{A}_{11}^{M_\theta} \pi^2 n^2) \cos \alpha + \frac{3}{2} \left(\left(\frac{1}{3} \pi^2 m^2 \bar{A}_{60}^{N_{x\theta}} + \frac{14}{9} \bar{A}_{20}^{N_\theta} \right) \sin \delta + \frac{4}{9} \bar{A}_{60}^{N_{x\theta}} \sin \alpha + \bar{R}_1 (\pi^2 m^2 \bar{A}_{60}^{N_{x\theta}} + \frac{14}{9} \bar{A}_{20}^{N_\theta}) \right) \cos^2 \delta + (m^2 \bar{A}_{20}^{N_\theta} (\bar{R}_1^2 + \frac{1}{3}) \pi^2 + \frac{26}{9} \bar{A}_{60}^{N_{x\theta}}) \sin \alpha + \frac{1}{3} \bar{R}_1 (m^2 \bar{A}_{20}^{N_\theta} (\bar{R}_1^2 + 3) \pi^2 + \frac{26}{9} \bar{A}_{60}^{N_{x\theta}}) \theta_0^2 \right) (-1)^m$$

$$L_{204}^5 = (\bar{h} (\frac{1}{2} (\pi^2 m^2 \bar{A}_{21}^{M_\theta} + \frac{26}{9} \bar{A}_{61}^{M_{x\theta}}) \theta_0^2 \cos^2 \delta + \theta_0^2 \bar{A}_{61}^{M_{x\theta}} (\pi^2 m^2 \bar{R}_1 + \frac{1}{3} \sin \alpha) \sin \delta + (\frac{1}{2} m^2 \bar{A}_{61}^{M_{x\theta}} (\bar{R}_1^2 + 1) \pi^2 + \frac{7\bar{A}_{21}^{M_\theta}}{9}) \theta_0^2 + \bar{A}_{11}^{M_\theta} \pi^2 n^2) \cos \alpha + \frac{3}{2} \left(\left(\frac{1}{3} \pi^2 m^2 \bar{A}_{60}^{N_{x\theta}} + \frac{14}{9} \bar{A}_{20}^{N_\theta} \right) \sin \delta + \frac{4}{9} \bar{A}_{60}^{N_{x\theta}} \sin \alpha + \bar{R}_1 (\pi^2 m^2 \bar{A}_{60}^{N_{x\theta}} + \frac{14}{9} \bar{A}_{20}^{N_\theta}) \right) \cos^2 \delta + (m^2 \bar{A}_{20}^{N_\theta} (\bar{R}_1^2 + \frac{1}{3}) \pi^2 + \frac{26}{9} \bar{A}_{60}^{N_{x\theta}}) \sin \alpha + \frac{1}{3} \bar{R}_1 (m^2 \bar{A}_{20}^{N_\theta} (\bar{R}_1^2 + 3) \pi^2 + \frac{26}{9} \bar{A}_{60}^{N_{x\theta}}) \theta_0^2 \right) (-1)^m$$

$$L_{204}^6 = (\bar{h} (\frac{13}{9} \bar{A}_{61}^{M_{x\theta}} \cos^2 \delta \theta_0^2 + \frac{1}{3} \theta_0^2 \bar{A}_{61}^{M_{x\theta}} \sin \alpha \sin \delta + (\frac{7}{9} \bar{A}_{21}^{M_\theta} + \frac{1}{2} \pi^2 m^2 \bar{R}_1^2 \bar{A}_{61}^{M_{x\theta}}) \theta_0^2 + \bar{A}_{11}^{M_\theta} \pi^2 n^2) \cos \alpha + \frac{1}{2} \bar{R}_1 \theta_0^2 (\pi^2 m^2 \bar{A}_{20}^{N_\theta} \bar{R}_1^2 + \frac{14}{3} \bar{A}_{20}^{N_\theta} \cos^2 \delta + \frac{26}{3} \bar{A}_{60}^{N_{x\theta}}) \theta_0^2) (-1)^n$$

$$L_{204}^7 = -\bar{h} (-\frac{7}{9} \theta_0^2 \cos^2 \delta (\bar{A}_{21}^{M_\theta} - \frac{13}{7} \bar{A}_{61}^{M_{x\theta}}) + \frac{1}{3} \theta_0^2 \bar{A}_{61}^{M_{x\theta}} \sin \alpha \sin \delta + (-\frac{1}{2} m^2 \bar{R}_1^2 (\bar{A}_{21}^{M_\theta} - \bar{A}_{61}^{M_{x\theta}}) \pi^2 + \frac{7}{9} \bar{A}_{21}^{M_\theta} - \frac{13}{9} \bar{A}_{61}^{M_{x\theta}}) \theta_0^2 + \bar{A}_{11}^{M_\theta} \pi^2 n^2) \cos \alpha$$

$$L_{205} = \frac{\theta_0}{4\pi^4 m^4} \left((-\pi^2 m^2 + \frac{1}{5} \pi^4 m^4 + \frac{3}{2}) \cos^4 \delta + (-\pi^2 m^2 \bar{R}_1 (\pi^2 m^2 - 3) \sin \delta - 3 - 2(\bar{R}_1^2 + \frac{1}{5}) m^4 \pi^4 + m^2 (3\bar{R}_1^2 + 2) \pi^2) \cos^2 \delta + 2\pi^2 m^2 (-\frac{3}{2} + m^2 (\bar{R}_1^2 + \frac{1}{2}) \pi^2) \bar{R}_1 \sin \delta + \frac{3}{2} + m^4 (\bar{R}_1^4 + 2\bar{R}_1^2 + \frac{1}{5}) \pi^4 + (-3\bar{R}_1^2 - 1) m^2 \pi^2 \right)$$

$$L_{206} = 0$$

Appendix B

The constant coefficients α_i for Eq. (49).

$$\alpha_1 = \frac{1}{L_{308}} \left(L_{309} K_p + L_{310} K_w + L_{306} (L_{102} L_{206} - L_{106} L_{202}) \frac{1}{L_{101} L_{202} - L_{102} L_{201}} - L_{307} (L_{101} L_{206} - L_{106} L_{201}) \frac{1}{L_{101} L_{202} - L_{102} L_{201}} + L_{301} (L_{102} L_{203} - L_{103} L_{202}) \frac{1}{L_{101} L_{202} - L_{102} L_{201}} - L_{302} (L_{101} L_{203} - L_{103} L_{201}) \frac{1}{L_{101} L_{202} - L_{102} L_{201}} + L_{303} \right)$$

$$\alpha_2 = \frac{1}{L_{308}} (L_{305} + L_{306} (L_{102} L_{203} - L_{103} L_{202}) \frac{1}{L_{101} L_{202} - L_{102} L_{201}} - L_{307} (L_{101} L_{203} - L_{103} L_{201}) \frac{1}{L_{101} L_{202} - L_{102} L_{201}} + L_{301} (L_{102} L_{204} - L_{104} L_{202}) \frac{1}{L_{101} L_{202} - L_{102} L_{201}} - L_{302} (L_{101} L_{204} - L_{104} L_{201}) \frac{1}{L_{101} L_{202} - L_{102} L_{201}})$$

HOW TO CITE THIS ARTICLE

V. Eslamdoust, H. Ahmadi, *Nonlinear Free Oscillation of Imperfect FG Porous Stiffened Open Conical Panels Resting on an Elastic Foundation under Thermal Conditions*, *AUT J. Mech Eng.*, 10(3) (2026) 389-416.

DOI: [10.22060/ajme.2026.25070.6247](https://doi.org/10.22060/ajme.2026.25070.6247)



